Budapest University of Technology and Economics
Faculty of Mechanical Engineering
Department of Fluid Mechanics

Utilizing parametric resonance to enhance the performance of a wave energy converter

BACHELOR'S THESIS

Author:
Assiya Syzdykova

Supervisor:
Dr. Josh Davidson
Research Fellow

Budapest, 2021

Declarations

Declaration of acceptance

This thesis fulfills all formal and content requirements prescribed by the Faculty of Mechanical Engineering of Budapest University of Technology and Economics, as well as it fully complies all tasks specified in the transcript. I consider this thesis as it is suitable for submission for public review and for public presentation.

Done at Budapest, 13.12.2019

Dr. Josh Davidson

Declaration of independent work

I, Assiya Syzdykova (SUCN7N), the undersigned, hereby declare that the present thesis work has been prepared by myself without any unauthorized help or assistance such that only the specified sources (references, tools, etc.) were used. All parts taken from other sources word by word or after rephrasing but with identical meaning were unambiguously identified with explicit reference to the sources utilized.

Done at Budapest, 13.12.2019

Assiya Syzdykova

Acknowledgments

I would like to express my deep gratitude to Dr. Josh Davidson, my research supervisor for his patient guidance, enthusiastic encouragement and useful critiques of this research work. When I started working on this problem, I had limited expirience on the practical use of phenomenon called parametric resonance. However, with assistance of Dr. Davidson, my knowledge on parametric resonance and its applicaliton with wave energy converters significantly expanded, that reflected on this thesis. I would also like to thank Dr. Tamás Kalmár-Nagy for sharing his insight on the Floquet theory and further assistance with handling it.

I would also like to extend my thanks to my family and fiance for their support and encouragement throughout my study.

Abstract

The wave energy conversion is a clean and inexhaustible energy source. However, under the current power performance level, the technology has to undergo some changes in order to be competitive. The conventional model of wave energy converter (WEC) is designed to resonate with the frequency of incoming waves. At resonance, the velocity of the system is in phase with the dynamic pressure and force of the wave, so that the amplitude of oscillations linearly increases, generating a massive amount of energy. As an alternative, the model can be oscillated by the periodic parameter with frequency twice its natural frequency. This practice stimulates an exponential increase in the amplitude of oscillations and explained by the phenomenon called parametric resonance. Parametric resonance could increase the amount of generated energy, and hence improve the performance of WEC. In this work, the phenomenon of parametric resonance is utilized on the single degree of freedom model mimicking a simplified WEC device. The model incorporates a mass modulation as a periodic parameter and exploits its effect on power performance. The parameters describing the model, such as damping and mass modulation coefficients have to be defined and optimized. Also, the long-term solution as stability diagram and Floquet theory is suggested to simplify the complexity of the non-linear model.

Keywords: *parametric resonance, mass modulation, WEC, stability, Floquet theory*

Contents

Nomenclature

This table summarizes the reoccurring abbreviations:

Notation	Name
DOF	degree of freedom
eq.	equation
OBC	oscillating body converters
ODE	ordinary differential equation
OWC	oscillating water column
PTO	power take-off
WEC	wave energy converter

This table summarizes the reoccurring mathematical terms and physical quantities with their names and units (if applicable):

Notation	Name [Unit]
λ	eigenvalue
μ	mass modulation coefficient [-]
ξ	damping ratio [-]
ρ	eigenvector
ϕ	phase change
ω	driving frequency [rad/s]
ω_d	damped natural frequency [rad/s]
ω_f	modulation frequency [rad/s]
ω_n	natural frequency [rad/s]
b	damping coefficient [Ns/m]
E	total energy [J]
F_{ex}	excitation force [N]
I	identity matrix
k	stiffness coeficient [N/m]
m_0	original mass of the system [kg]
P	power [W]
T	period of the system [s]
T_f	period of the time-varying parameter [s]

Introduction

Wave energy is a renewable energy source with a huge potential for sustainable growth. It is a complex field with a lot of rooms for improvement. The improvement can come in many forms, the trivial solution is the size optimization of wave energy converters (WECs) described in [1–3], another is to detect and suppress negative instability effects [4] or create tuning mechanism [5–7] to heave the oscillating body in irregular seas. In addition, prediction of available wave energy flux along with other factors (such as weather conditions, economic profitability) is vital for the design and deployment of dedicated devices [8]. In order to succeed, a better understanding and exploitation of the device's nonlinear hydrodynamic model can prove beneficial to the optimization and improvements of the potential concepts. In this work, an utilization of the parametric resonance (from nonlinear dynamics) with time-varying inertia and its effect on the power output of the oscillating WECs is under study.

There are two distinguishing types of oscillatory responses: forced oscillations and parametric oscillation. Forced oscillations appear if dynamical body is excited by a time-varying external force input; and if frequency of such input close to the natural frequency of the body, the body will be subjected to resonance. This phenomenon causes linear increase in oscillation amplitude and wildly exploited in oscillating WECs. On the other hand, if the body has periodic parameter(s), it will result in parametric oscillations; and if frequency of periodic parameter is about twice the natural frequency, the body will experience parametric resonance. The concept of parametric resonance was discovered in the 19th century and mainly applied (in a negative connotation) to the ships' motion [9]. Further research [10] showed the mechanical amplification (in the system's response) associated with parametric excitation. Due to parametric resonance, the amplitude of vibration increases exponentially. This fact changed the perception of parametric resonance and stimulated further developments of mechanisms triggering instability, known as parametric resonance.

The oscillating WECs are the vibrating devices, capturing power stored in ocean waves. The power rate is proportional to the amplitude of the oscillations, which is why in 2007 it was suggested to apply parametric resonance to improve the performance of oscillating water column (type of WEC) [11]. Later this work was refined by Orazov et al [12, 13], suggesting a novel excitation schemes. Both works show a significant boost in power output.

One of the distinct parameters in the WECs is mass. Due to exposure to the ambient water, the system has an infinite theoretical stock of unused mass. This additional mass can be seized and released at any time. If the mass is trapped and releases periodically as a function of time, under certain circumstances, it could lead to parametric resonance in the system. To discover those circumstances a single degree of freedom model close to the dynamics of WEC was studied. A simulation considers an idealized case of a simple mass-spring-damper model with a harmonically varying mass value. The behavior of the dynamic system is described by the second-order differential equation with a periodic coefficient, similar to the Mathieu equation, but instead of periodic restoring force, focused on a time-varying inertia value, which has been termed by the Carson-Cambi equation. The mass modulation is described as the percentage of the original mass and provides the internal

excitation to enable the occurrence of parametric resonance. The velocity, average power output, and total energy at the different modulated mass values and modulation frequencies are recorded and used for analysis. The system will be examined by simulating the model using numerical integration methods. Then, from the analysis of the non-linear dynamics, the Floquet theory and Poincare Maps will be used to identify the possible regions of instability and determine a long-term approach in parameter settings.

It is expected that a higher mass of the system gives higher power output. However, considering the realization expenses of mass modulation in WECs, the manufacturers are going to face the trade-offs between the power output and the cost. It is important to determine the relationships between the mass variation and the output power along with the optimal compromise between increased energy extraction and practical engineering considerations. We are planning to compare the accuracy of computed theoretical results to the realistic scenario, determining the limits of an actual structure. Discussing size optimization is essential for the successful development of the wave conversion industry.

Outline and objectives

The objective of this work is to present optimal mass-modulation parameter values from power output perspective as well as from techno-economic sizing. The theoretical approach of instability regions have to be verified with numerical simulation for dedicated quantities. Introduction to a wave energy conversion and mass-modulation schemes presented in Chapter 1. Next, the phenomenon of parametric resonance and parametric resonance carrying equations will be exploited in Chapter 2. Utilization of Floquet theory in order to determine instability regions as a possible replacement to a long-running numerical simulations proposed in Chapter 3. The details of the test case, implemented numerical simulation's values and stability theory will be carried in Chapter 4, along with results on the performance of the system. Finally, a number of conclusions will be drawn in Chapter 5.

1 Conversion of the ocean energy

The world energy consumption considerably raised over the last decades and is expected to continue growing. The increasing demand reflects possible changes in the composition of the economy, such as shifts to more energy-intensive industries and developing alternative inexhaustible energy sources [14]. Ocean energy is highly predictable and is well suited to provide baseload power [15]. The theoretical resource potential of ocean energy is sufficient to meet present and projected global electricity demand well into the future [15, 16]. Although the ocean energy technology is relatively new, and currently not economically competitive with more mature technologies such as wind energy or solar energy, the interest from governments and industry is steadily increasing [17].

1.1 Wave energy conversion

Ocean energy is complex and versatile. It is the most concentrated form of renewable energy[1] on earth [18]. Ocean energy can be acquired in different forms, such as thermal, mechanical, or chemical energy. The energy we will discuss in this thesis is the mechanical energy. Mechanical energy of the ocean is associated with generated wind on the surface of the ocean leading to the formation of the waves; and the gravitational force of the moon that affects the tides.

A device that transforms kinetic and potential energy contained in ocean waves into useful mechanical, later electrical energy called wave energy converter (WEC). The history of WECs is dated back to 1799 when Pierre-Simon Girard invented the first known device that uses energy from ocean waves to operate the pumps and other machinery on ships [17]. More than a century later, Bochaux-Praceique constructed a device that uses wave energy to light and power his house at Royan, France [19]. It was the first oscillating water-column type of wave-energy device. Although the concept of wave power has been around for at least two hundred years, the significant attention towards the idea of wave energy conversion gained only in the 1970s. The limited stocks of fuel caused prices to rise, as well as the appearance of ecological and environmental problems associated with unregulated and uncontrolled fuel consumption forced people to develop alternative energy sources [16, 19, 20].

Renewable energy supports a wide range of socio-economic benefits, including new opportunities for economic activity, local value creation, job creation, improved livelihoods, gender equity and more [15]. WECs produce no gaseous, liquid or solid emissions and hence, in normal operation, wave energy is virtually a non-polluting source [21]. However, the environmental impact from deployment of wave power schemes is varying: some of the effects may be beneficial and some potentially adverse. Nonetheless, the interest in a development of wave power is constantly increasing and can be summarized in the United Nations Secretary-General António Guterres statement: "Oceans, seas and marine resources are critical to sustainable development, including sustainable ocean-based economies and to the 2030 Agenda for Sustainable Development as a whole. They underpin poverty eradication

[1] solar energy has a density of 1.5 $\mu J/m^3$, wind energy - 0.5 J/m^3, meanwhile the wave energy density is 50 J/m^3

and food security, are a source of employment and livelihoods and support the well-being of humans and the planet" [22].

Wave energy takes a share of up to 80% of ocean energy and considered the most promising type, it is widely available around the world [23]. The energy density contained in waves is the highest among the renewable energy sources [18, 24]. Waves are generated by winds, which in turn are generated by solar energy; and while wind and solar power devices generate power around 20-30% of the time, the wave power devices produce it up to 90% [25]. Moreover, the solar energy intensity of typically 0.1-0.3 kW/m^2 on horizontal surface is converted to an average power flow with intensity of 2-3 kW/m^2 on a vertical plane perpendicular to the wave direction [26]. The power in a wave is proportional to the square of the amplitude and to the period of motion. Therefore, long period ($\sim$ 7–10 s), large amplitude ($\sim$ 2 m) waves have energy fluxes commonly averaging between 40 and 70 kW/m widths of oncoming wave. Nearer the coastline, the average energy intensity of a wave decreases due to interaction with the seabed [17]. The location of the WEC devices is usually between 30° and 60° latitude and in deep-water below 40 meters. The WECs can provide clean energy to power the electrical grid as well as many other applications such as propulsion for ocean vehicles or pumping for seawater desalination [27]. The estimated power of WECs is around 32,000 TWh/year, having the potential to reach 80,000 TWh/year [25, 28, 29]. Advancing the theoretical power output can be especially useful for temperate climate regions directly exposed to the sea or ocean since the natural seasonal changeability of wave energy is following the electricity demands in that climate region and can replace all alternative energy sources [17].

Nowadays, a broad variety of WEC designs and concepts exist in a different stages of development. The classification of WECs can be done in multiple ways; in [30] three main categories are distinguished (Figure 1): (a) *oscillating water columns* that use trapped air pockets in a water column to drive a turbine, (b) *oscillating body converters* that are floating or submerged devices using the wave motion (up/down, forwards/backwards, side to side) to generate electricity, and (c) *overtopping converters* that use reservoirs to create a head and subsequently drive turbines. In addition, each category can be subdivided according to the operation principle[2] (rotation/ translation), their power takeoff system (air turbines, hydraulic turbines, hydraulic engines), their positioning within the ocean (shoreline, near shore, off shore), and their directional characteristics (fixed, floating, submerged).

The power take-off system (PTO) is a method for extracting power from a power source. PTO is affecting the overall performance of WEC to deliver desired electrical energy and the cost of the device [24]. Essentially most of the energy ($\sim$95%) contained in waves is located between the water surface and top 1/4 of the wave length [30]. The extraction of this energy would depend on the PTO technology. The overtopping converters have a similar operation to the small conventional hydroelectric power sources, therefore they can use the same low head hydro-kinetic turbines for their PTO. The main challenge of oscillating water columns and oscillating body converters is conversion of low-velocity motion of the device itself to unidirectional motion by the PTO system. As a result, OWCs use air turbines for their PTO, and OBCs utilize piston-like systems, such as hydraulic/mechanical drives, gas accumulators, or direct drive linear generators. More detailed information can be found in [31, 32]. In the

[2]the technology that converts wave energy into pneumatic/mechanical energy

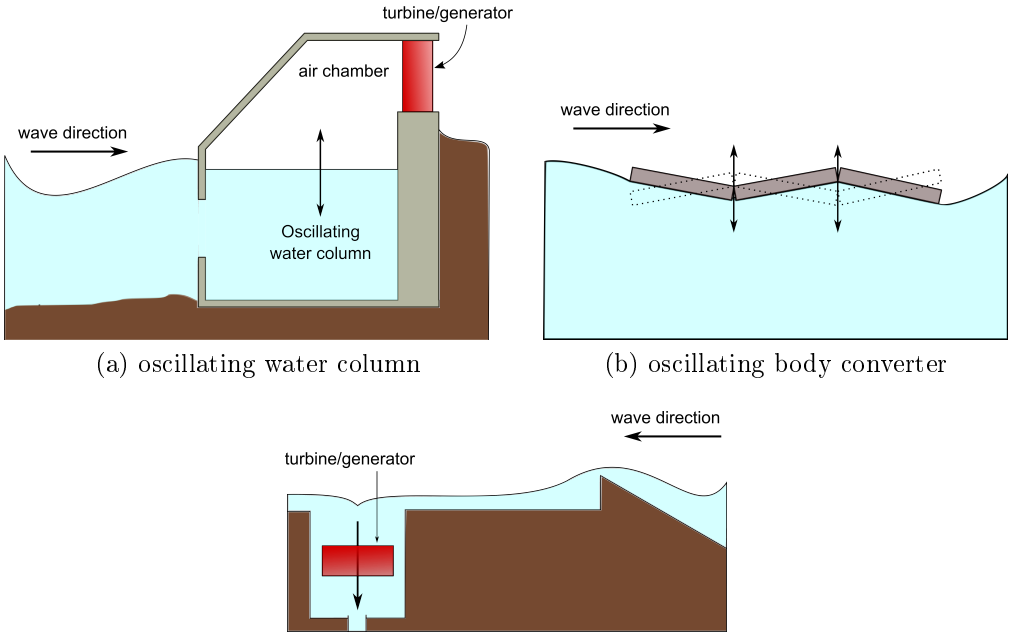

(a) oscillating water column

(b) oscillating body converter

(c) overtopping converter

Figure 1: Conceptual drawing of a different class of WECs

review on power performance and efficacy its been reported that oscillating body converters have the highest efficacy per characteristic width[3] ratio, and overtopping converters have the lowest [24]. The same report states that oscillating water columns and oscillating body converters tend to perform better when the wave energy potential increase, while overtopping converters seem to perform irrespective of the amount of wave energy potential. That could be explained by the fact that the device's energy harvesting capabilities depend on wave amplitude and the difference between the turbine and the height water storage.

The primary type of WEC of interest are oscillating body converters (OBC). Those devices convert the wave force into oscillatory motions, and then the PTO system utilizes the motion to drive a generator [12]. The device of such kind is an attenuator. It is a long floating device placed parallel to the predominant wave direction that is operated in offshore locations. It consists of multiple segments (arms) connected by joints together and the energy generated due to the relative motion of hinged arms as the wave passes by. The articulated joints contain piston-cylinder arrangements whose relative movements pressurize hydraulic fluid that drives a motor connected to a generator. The generated electric power is transmitted to shore by using subsea cables. [8,33] The movements along the prevalent length can be selectively constrained to capture more energy. One of the most known attenuator type is the Pelamis device (Figure 2), a semi-submerged articulated structure composed of cylindrical sections linked by hinged joints. The wave induced motion of these joints is resisted by hydraulic rams which pump high pressure oil through hydraulic motors via smoothing accumulators. A 130 m long and 3.5 m diameter device rated at 375 kW is being developed by Ocean Power Delivery [34,35].

[3]the part of the device that is in contact with ocean wave

Figure 2: Pelamis Wave Energy Converter
Source: `http://www.emec.org.uk/about-us/wave-clients/pelamis-wave-power/`

Another common type of WEC that will be discussed is an oscillating water column (OWC). It consists of a semi-submerged chamber opened to the sea below the waterline, and with the air is trapped in a pocket above the waterline. With the wave approaching the device, the water is forced into the chamber, creating pressure on the air within. This air is escaping to the atmosphere through the turbine. Then, the turbine is driving air back when the water retreats. This continuous movement generates a reversing stream of high-velocity air, which is channeled through a rotor-blades turbine to produce electricity [30]. For this applications, a low-pressure Wells turbine is often used, as it rotates in the same direction independent of the flow direction, which removes the need to rectify the airflow [27]. The main advantage of OWC is its simplicity and reliability, and the drawback is its low-performance level, therefore the new control strategies and turbine concepts are under development [30]. For instance, in order to increase performance, a new generation of floating OWC are integrated on spar buoys. The environmental impact of OWC is mainly positive. Essentially there are no moving parts of OWC other than the air turbine therefore sea life is not damaged, on a contrary, supported, as OWC creating an artificial reef. One of the significant OWC power plants is LIMPET. Opened in 2001, this power plant generates 500 kW with a single 2.6-meter diameter Wells turbine connected to a collecting chamber made up of 3 connected tubes measuring 6x6 meters [36]. The LIMPET was constructed by Queen's University Belfast in partnership with Wavegen Ireland Ltd.

1.2 Limitations of current wave power technologies

Due to the limited commercial experience, the current techno-economic performance of WECs is not competitive compared to other renewable technologies. The industry needs considerable research to make WECs economical without losing its performance, this has to be done in an environmentally beneficial and economically reasonable scheme. To be competitive, the design of a WEC has to efficiently cope with several difficulties, such as a corrosive environment, immense loading in extreme weather conditions, randomness in power input and low transmission frequencies [3, 17].

One of the significant challenges is the conversion of the slow ($\sim$ 0.1 Hz), random, high-force frequencies into useful motion to drive a generator with output quality acceptable to the utility network. As waves vary in amplitude and period, their respective power levels vary accordingly. Whereas gross average power levels can be predicted in advance, this variable input has to be converted into smooth electrical output and hence requires some type of energy storage system, or other means of compensation such as an array of

devices [27]. Moreover, the direction of the waves in offshore locations is highly alternating. To capture the energy of wave the device has to align accordingly on compliant moorings. Using the phenomenon of refraction[4] and reflection[5] we can largely determine the directions of waves near the shore. The irregularity in wave amplitude, phase, and direction significantly complicate the design of the device, yet another challenge is to mitigate the highly corrosive environment of devices at the water surface [24, 37].

To operate efficiently, the device and corresponding systems have to be rated for the most common wave power levels (∼30–70kW/m), as well as withstand extreme wave conditions that occur very rarely, but could have power levels in excess of 2000 kW/m [27, 38]. The economic dilemma comes from the fact that whilst the normal output of the device (and the revenue) produced by the most commonly occurring waves, the capital cost of the device construction is driven by a need to withstand the high power level of the extreme, yet infrequent, waves [39]. The device based on nominal operating conditions is cheaper, but its life expectancy is shorter compare to more costly WEC that could withstand severe conditions. The problem of the design choice could make the WEC an economic failure [37].

We also have to keep in mind that, whereas small-scale wave energy plants are likely to have minimal environmental impacts, some of the very large-scale projects that have been proposed have the potential for harming ocean ecosystems. Covering very large areas of the surface of the ocean with wave energy devices would harm marine life and could have more widespread effects, by altering the way the ocean interacts with the atmosphere. Wave power plants act as wave breakers, calming the sea. While this is often a desired effect in many harbors the result may be to slow the mixing of the upper layers of the sea which could adversely impact marine life and fisheries [25].

1.3 Mass-modulation in wave energy devices

As was mentioned before, the current techno-economic performance of WECs has to be improved in order to compete in the market. It is believed that taking advantage of surroundings, more precisely the ambient water holds the opportunity to enhance the energy harvesting capabilities of WEC devices. The implementation, as mass-modulation schemes, is a relatively new concept first introduced by Orazov et al in [12] and continued in [13, 40]. The proposed excitation schemes extend the idea of applying the mass of surrounding water as ballast, and in addition, produce mechanical amplifications[6].

The wave excitation schemes could be linked to the parametric excitation of an oscillator. The seminar paper by Rugar and Gütter [10] describes how parametric excitation can produce mechanical amplification in response to resonator. This amplification has been already implemented in variety of microelectromechanical system oscillators, detailed in [41–43], and explored for OWC devices in [11]. The novel excitation scheme proposed by Orazov et al mimics a square wave modulation of the mass of OBC devices, such as Wavebob and Pelamis.

[4] as the wave travels from deep into shallower water near the shore, it is refracted from its original direction of travel to an angle more normal to the shoreline

[5] the wavelength of the water wave gets shorter proportional to the wave fronts proximity

[6] increase in magnitude of mechanical quantities

The mass intake machanism is normalized against the occurring wave's period and consists of 4 steps: the system traps the water at the first quarter of a period and releases it at the second quarter of a period; then the system traps the water again at the third quarter of a period and releases the water once more at the fourth quarter of a period [12]. This changes in a water level can be described with sinusoidal wave. The figure below (Figure 3) illustrates the typical period of the water intake system's motion:

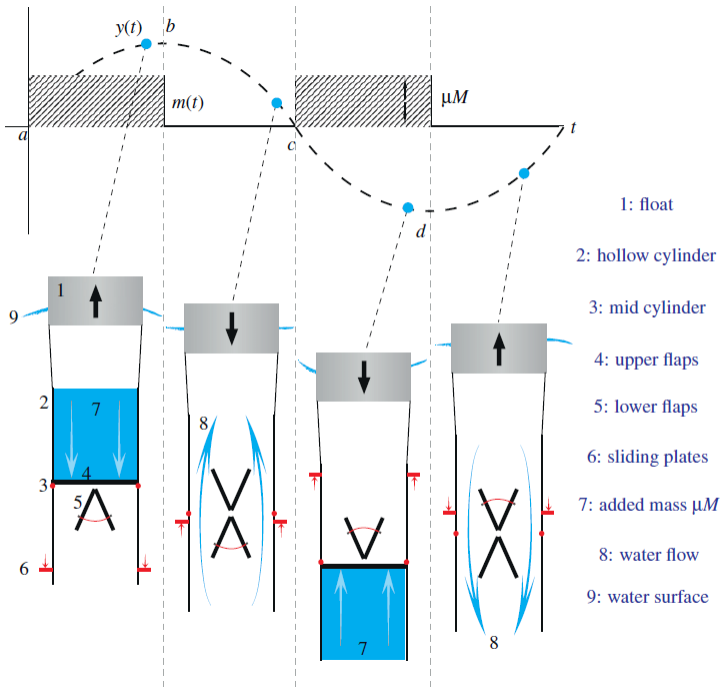

Figure 3: Illustration of the operation of the water intake mechanism
Source: `http://me.berkeley.edu/~bayram/wec/water_intake_animation.html`

The system in Figure 3 is composed of exposed at both ends, constantly submerged hollow cylinder (2) fixed to the surface float (1) that is excited by upcoming waves. In the middle point of cylinder (3) two pairs of butterfly flaps (4) and (5) are hinged. The lower pair of flaps (5) can only move from horizontal ("closed") to nearly vertical down ("open") position, while upper pair of flaps (4) only move from horizontal ("closed") to nearly vertical up ("open") position. There is also a horizontal plate (6) outside of the cylinder sliding up and down due to the water pressure and depending on the wave's motion. As the plate passes midpoint (3) it can lock or unlock the flap pair in open position. The red arc on the flaps indicate locked pair. The mechanism is arranged to hold at most one set of flaps in closed (unlocked) position. The added mass (7) termed μM is the mass of the system M multiplied by the mass coefficient μ, where μ could be any number between 0 and 1. The flow of the incoming water (8) is pictured by the stream lines and the surface level of the ambient water (9) is depicted by the cosine wave.

At point (a) at the graph on top in Figure 3 the sliding plate (6) goes below the midpoint (3) as the water amplitude (9) is at its highest, locking lower pair of flaps (5) in the open position and unlocking upper pair (6). As the system moves up (along with wave), the upper flaps (4) will slide downward (to complete closed position) due to the higher pressure above them than below. The water will be trapped in the upper part of the cylinder, causing added

mass effect.

At point (b), the direction of motion is reversed. As the water amplitude is decreasing, the entire system is accelerating downwards. The sliding plate (6) is moving up relative to the cylinder, but the lower flaps (5) are still locked until point (c) of a cycle. The upper flaps (4) slide up due to higher pressure below them, allowing the water to pass down.

At point (c), the mechanism continues to accelerate downwards, along with the wave amplitude, reaching its maximum vertical velocity. The plate (6) moving upwards, locking upper flaps (4) and unlocking lower flaps (5). The lower flaps (5) take horizontal (closed) position due to pressure different blocking water in the lower part of the cylinder (2), leading to the effect of the added mass. The plate (6) reaches a completely up position at a point (d).

At point (d), the system starts accelerating upwards and the wave amplitude is increasing as well. That causes lower flaps (5) to open and the upper flaps (4) are still locked by the plate (6). The water passes through the system, removing any additional mass. The sliding plate moving down relative to the cylinder (2) reaching middle (3) at the point (a) of the next cycle.

Note that the sliding plate (6) is acting inertial, it is moving relatively the cylinder while its absolute position remains nearly stationary. Those mass excitation schemes are applicable for the devices suitable for active changes in a mass (and thus natural frequency). The water intake and disposal would happen rapidly twice per cycle. The intake is happening at points (a) and (c), while disposal at points (b) and (d). The cycle keeps repeating. In his early work [12], Orazov et al analyzed the simple one degree of freedom model. Later the two degrees of freedom simulation was performed in [44]. Both simulations showed improvement of power with growth of the mass modulation coefficient μ and at the optimal damping. However, further increase of mass modulation coefficient comes at the cost of increased system complexity and possible impulse loading at instances where the mass changes [44].

2 Mechanics of wave energy converters

This chapter is dedicated to providing the necessary theoretical knowledge along with used mathematical equations to build the numerical simulation. The main focus is to explore the phenomenon of parametric resonance and determine the governing equations for the system.

2.1 Power output

The significant factors in the prevalence of one WEC device over another are its efficacy and the power output. The efficacy of the system is the ratio of absorbed power and power available within device width. The number mostly depends on the type of WEC, such that the device with the higher width in contact with ocean wave is going to be at a disadvantage compared to a shorter-width WEC absorbing the same amount of power.

The second characteristic value is the captured power rate. Power is a scalar quantity defining the amount of energy converted per unit of time. The general definition of power:

$$P = \frac{dW}{dt} = \frac{d}{dt}(Fx) \tag{1}$$

where power P is the rate of work done W with respect to time t, whereas the work can be described as a product of force F and the displacement x. From the fundamental theorem of calculus, the equation (1) can be simplified to:

$$P = Fv \tag{2}$$

where F is force applied at the system and v is the velocity in the direction of applied force.

Due to the periodic excitation, the velocity (and, hence, power rate) will vary within a cycle, as a result, instead of normal power (1) average power[7] will be used:

$$\overline{P} = \frac{\Delta W}{\Delta t} = \frac{1}{n}\sum_{i=1}^{n} b_n v_n^2 \tag{3}$$

The equation (3) is pointing out the dependency of power on damping b and velocity v of the body. This last part of the equation derived from the fact that in many vibrating systems the frictional force F_f defines the power rate and it's proportional to the product of damping coefficient b and velocity of the system v:

$$F_f = bv \tag{4}$$

Whereas efficacy depends on the sizing of the WEC device, the power output could be improved using the solution provided in Section 2.2.

[7] power averaged over a cycle

2.2 Parametric resonance

The peak performance of most oscillating water columns (OWC) occur at the frequency resonant with incident wave frequency, so that the velocity of an oscillating body is in phase with the dynamic pressure and force of the incoming wave [11]. This results in substantial transfer of energy from the incident wave to the device. At resonant frequency oscillations tend to increase linearly within time until damping suppresses further growth. This makes resonance a desirable feature for many PTO systems. For the oscillating body converters (OBC) whose model is under study, the efficacy of the energy absorbed can be significantly improved too, when the system is at resonance with incoming wave [24]. However, if the system is excited at the parametric resonance, it has oscillations increasing exponentially. Compare to normal resonance, this phenomenon received far less attention, that could be explained by the complexity of mathematical models of non-linear problem [4].

Resonance

Every system has a certain frequency at which in absence of any driving force or damping it tends to oscillate freely. The frequency of this vibrations is called natural frequency. The oscillation of a free vibrating[8] system is recessed due to damping. It is a dissipation of energy stored in oscillation due to internal friction of surrounding air molecules. If a periodic force applied to the system, it's called forced system [45]. The forced system starts to oscillate with the frequency of applied force, and continue unless applied force is removed. A resonance is the phenomenon that occurs when the frequency of a periodically applied force is close or equal to a natural frequency of the dynamic system and leads to an increase in amplitude. The resonant frequency is a frequency at which the amplitude's magnitude is at its relative maximum. Due to the storage of vibration energy, even small periodic forces close to the system's resonant frequency are capable of producing high amplitude oscillations. Essentially, resonance is mechanism that generates practically all sinusoidal waves and vibrations.

The resonance occurs extensively in nature and is exploited in many engineering fields, for instance to generate vibrations of a specific frequency in musical instrument. Many sound we hear, like the struck of hard objects such as metallic, glassy or wooden, are caused by resonant vibration within an object. Resonance can be observed at the playground swings, which act as a pendulum. If a swing is pushed multiple times with the period equal to the natural interval of the swing (its resonant frequency), the swing will go higher and the amplitude will keep increasing due to the maximized energy absorption by a swing. If pushing will be slower or faster than the natural interval of the swing, the produced arc will be smaller and the amplitude will decrease.

Consider externally excited damped mass on a spring. The system in Figure 64 is one degree of freedom system subjected to harmonic excitation.

The behavior of this system can be characterized by the Newton's second law in a form:

$$m\ddot{x} + b\dot{x} + kx = F_{ex} \tag{5}$$

[8] no external force to drive the system

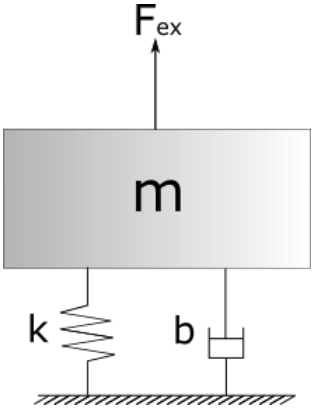

Figure 4: Spring-mass-damper system

where m is the mass, b is the viscous damping, and k is the spring's stiffness of the system. The displacement of body m described by x is going to be back and forth repeatedly about its mean position. This repetitions come in the regular interval T and characterized by the natural frequency of the system ω_n:

$$T = \frac{2\pi}{\omega_n} \tag{6}$$

Note that the natural frequency of damped and undamped systems vary. The displacement from the equilibrium point derived with respect to time gives velocity of the system $\dot{x} = \frac{dx}{dt}$, and its acceleration $\ddot{x} = \frac{d^2x}{dt^2}$. The system is driven by externally applied sinusoidal force:

$$F_{ex} = F_0 \sin(\omega t) \tag{7}$$

where F_0 is the driving amplitude and ω is the external forcing frequency.

In Figure 5 the displacement of the system (4) is depicted. In the first frame we can see 2 characteristic oscillations: damped ($b \neq 0$) and undamped ($b = 0$). Both oscillations belong to free vibration system ($F_{ex} = 0$). The blue line shows the undamped system oscillating with it's natural frequency (ω_n):

$$\omega_n = \sqrt{\frac{k}{m}} \tag{8}$$

The amplitude[9] of oscillations remains constant as $t \to \infty$. While, in case of damped unforced system (red line) the oscillations are decaying, hence the amplitude is decreasing after each period approaching zero as $t \to \infty$. The intensity of the decay depends on damping coefficient: the system with higher damping tend to decay faster. The damping can be rated with damping ratio:

$$\zeta = \frac{b}{2m\omega_n} \tag{9}$$

If $\zeta = 0$, the system is undamped, and if $0 < \zeta < 1$, system is going to have dumped vibrations. If $\zeta \geq 1$ the system will be overdamped. Overdamped system would not show any oscillations due to fast energy dissipation. The natural frequency of system with damper depends on undamped natural frequency and damping ratio:

$$\omega_d = \omega_n \sqrt{1 - \zeta^2} \tag{10}$$

[9]largest deviation from equilibrium point (peak)

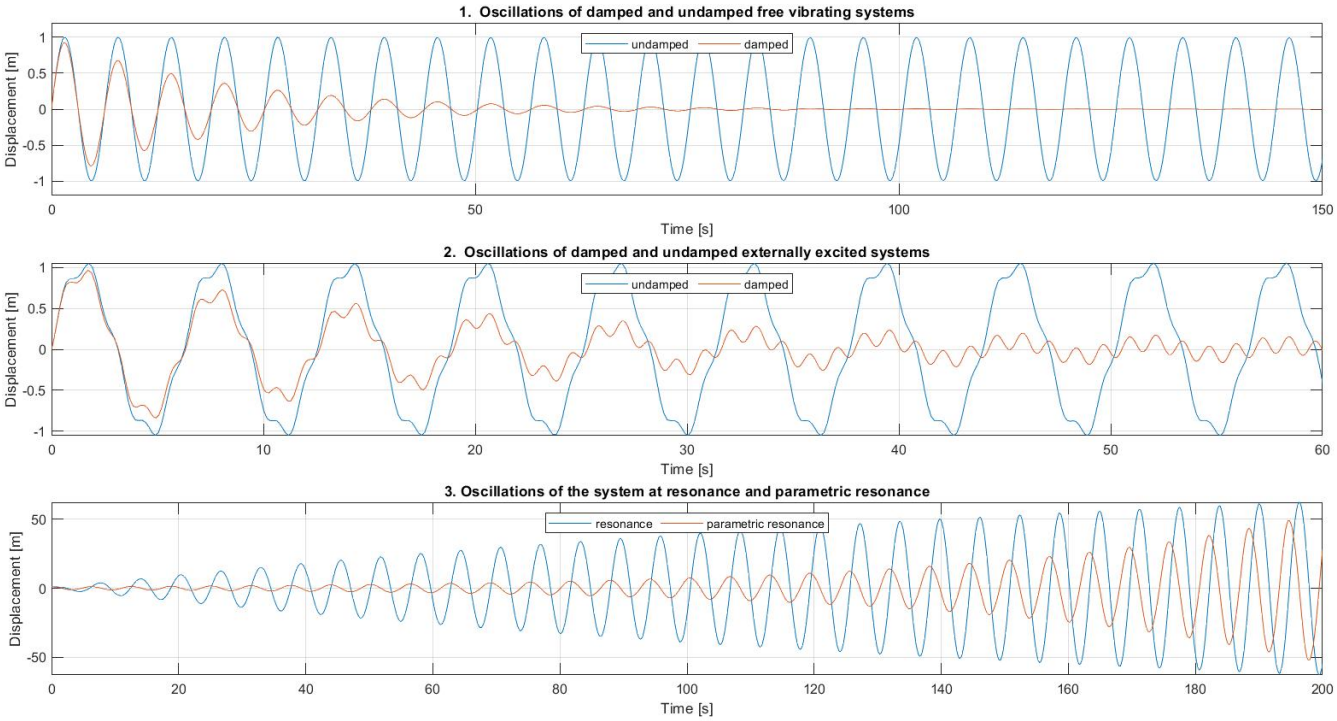

Figure 5: Different types of oscillatory behavior

The second frame (Figure 5) shows the behavior of externally excited system with and without damping. Forced oscillations occur when an oscillating system is driven by a periodic force that is external to the oscillating system [46]. The response to the imposed driving depends on driving amplitude and driving frequency. Forced system has two oscillations combined: due to natural frequency and due to forcing. Without damping (blue line), the behavior of forced system is similar to free vibration system (has no decay). Although, the displacement (and amplitude) will be higher due to external excitation. The displacement of the forced system with a damper (red line) decreases, since the vibrations due to natural frequency getting absorbed by a damper. But, if the damping ratio (ζ) is between 0 and 1, the oscillations remain: after vibration due to natural frequency dissolves, the system keeps oscillating by external excitation at the forcing period.

The last frame in Figure 5 illustrates the resonance. The system has natural frequency ω_d and it is externally excited by F_{ex}. If the forcing frequency close or equals to natural frequency ($\omega \cong \omega_d$) the response of this system is shown with blue line. The oscillations of such system are growing *linearly* in time due to resonance. However, what will happen if the system is excited by a time-varying parameter, such as $m(t)$? This practically means that mass of the system is a function of time. And, under certain conditions we could achieve *exponential* growth in oscillations shown with the red line.

Parametric resonance

Parametric resonance is an instability phenomenon caused by time-varying changes in the parameters of the system [47]. The equation of motion of such system will be:

$$\begin{aligned} m(t)\ddot{x} + b\dot{x} + kx &= 0, \text{ or} \\ m\ddot{x} + b(t)\dot{x} + kx &= 0, \text{ or} \\ m\ddot{x} + b\dot{x} + k(t)x &= 0 \end{aligned}$$

where parameters $m(t), b(t), k(t)$ depend only on time, and not on the state of system. This parameters will vary periodically with the period T_f, and if its frequency ω_f:

$$\omega_f = \frac{2\pi}{T_f} \tag{11}$$

close or equals to twice the natural frequency ($\omega_f \cong 2\omega_n$), the system phase-locks to the parametric variation and absorbs energy at a rate equivalent to the energy it already has. Without compensating energy-loss mechanism, provided by damper b, the amplitude of oscillations will grow exponentially, as shown in Figure 6:

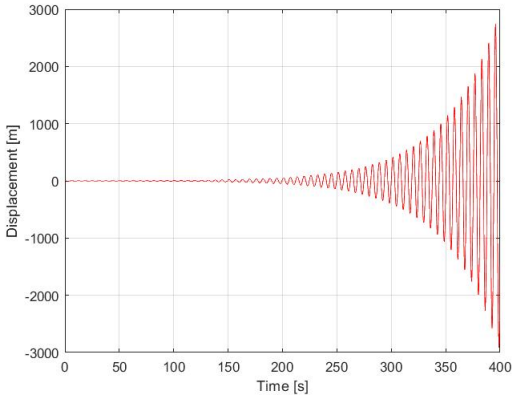

Figure 6: Oscillations of system (4) at the parametric resonance

The first to notice that the system excited by force of double its frequency was Michael Faraday in 1831. His work [48] studied crispations[10] in a open container partially filled with liquid and excited vertically to generate waves with frequency half the driving frequency. The variation in system's parameters comes from changing wetted surface (of container) due to approaching ripples. Another observation was maid by Froude [9]: the ship sailing in a ocean produce a roll motion, and can be parametrically excited by the other motions in a ship. The roll angle increases rapidly if the period of the ship is in resonance with a period of incident waves, and the ship experiences so-called parametric roll. Parametric roll is a type of parametric resonance, when the large oscillations come in roll motion [47]. Parametric resonance is detrimental for the ships, it could endanger the ship, its crew, and the cargo. Nowadays, there are examples of accidents with container vessels that caused damage worth millions of euro's [49, 50], such as APL China (1998), Maersk Carolina (2003) and etc. The World Shipping Council estimates the loss of around 1000 containers per year

[10] ripples on a wave surface

due to parametric rolling motion [51]. More misfortune would be a cruise ship experiencing parametric resonance, since the cost will be human lives. Thence numerous studies are devoted to detect and suppress the parametric resonance, such as [47, 49, 50, 52–54].

Similar to the ships, the other offshore floating structures are subjected to effect of parametric resonance. The influence can be positive as well as adverse. There are works describing the negative effect of parametric resonance in WEC [4, 55–57], since the energy in primary motion mode transfers into other modes, resulting in less available energy for conversion. Whereas, other papers feature positive effect of parametric resonance on the power performance of the WEC (for instance, [11–13, 40] and the references therein).

While the conventional oscillating WEC were designed to resonate with the peak frequency: such resonance would cause a linear increase of oscillation amplitude, the mass modulation technique triggers parametric instability, causing the parametric resonance. The [11] features the effect of parametric resonance on performance of OWC. The incident water acts as a natural excitation of the device, since it generates a periodic pressure signal at the lowest point of the body. The effect of this water can be viewed as forced oscillation. The alternative way suggested by [11] is to excite mechanical model by periodic variation in parameters which describe such model. Out of all the parameters, it appeared the most practical to vary the volume of the device. The way how mass modulations take advantage of the fluid environment and incident waves can be viewed as a form of parametric excitation [40]. The occurrence of parametric resonance leads to an exponential increase of oscillation amplitude, providing the possibility to extract additional power. In [11] the mass alternation happens in the two-quarter cycles (four times), featuring the system with trapped ballast at the beginning of the period and the descending water level to its equilibrium level at the first quarter of the period. The system starts trapping the ballast once more reaching an absolute at the end of the second quarter. Then, the process repeats. At the end of the period, the water level reaches its initial value. The proposed mass-modulation is different from the one used within this work mainly by the initial state of the mass of the device, that could be explained by the choice of different WEC model. The results of [11] show that the energy is transferred more efficiently by the parametric resonance rather than due to external excitation. The exponential growth of the amplitude provides instant response for any initial perturbation and the actual maximum amplitude is greater than the actual amplitude of the system subjected to resonance.

In works [12, 13], Orazov et al used numerical simulations to determine power improvement. The defining arguments were the damping b and mass modulation coefficient μ. However, the mass modulation frequency was not taken into consideration. This work is going to feature the Mathieu and Carson-Cambi equations that will denote the periodic parameter defined by mass modulation coefficient and mass modulation frequency.

2.3 Mathieu Equation

When one encounters with parametric resonance in a body, the Mathieu's equation is useful tool to understand its mathematical model [47]. The Mathieu's equation is a second order differential equation introduced by Émile L. Mathieu in 1868 [58]. This equation describes

the vibrational movement in the stretched membrane with elliptical boundary [59]. When transforming the two dimensional wave equation

$$\frac{\partial^2 V}{\partial x^2} + \frac{\partial^2 V}{\partial y^2} + c^2 V = 0 \tag{12}$$

into elliptical coordinates, the Mathieu differential equation was obtained:

$$\frac{d^2 x}{dt^2} + (a - 2q\cos 2t)x = 0 \tag{13}$$

where a and q are the real coefficients.

The Mathieu equation describes a wide range of phenomena in nonlinear vibration theory. Various mechanical and structural dynamical systems described by elliptical geometry can be accurately and realistically modeled; including wave propagation in pipes, oscillation of water in a sea, and in floating vessels [60].

The boundary condition of the equation (13) reflects the periodic nature of the trigonometric term $\cos 2t$:

$$x(t) = x(t + \pi), \tag{14}$$

Nowadays, we are using simplified version of equation (13) in a form:

$$\ddot{x} + (\delta + \epsilon\cos\omega t)x = 0 \tag{15}$$

where δ and ϵ are the real coefficients, and the term $\cos\omega t$ is a parametric excitation. This linear differential equation commonly occurs in nonlinear vibration problems in two different ways: (i) in systems with periodic forcing and (ii) instability studies of periodic motions in nonlinear autonomous systems [61].

An example of (i) is a pendulum with support periodically forced in a vertical direction (Figure 7a), that has governing differential equation:

$$\ddot{x} + \left(\frac{g}{L} - \frac{A\omega^2}{L}\cos\omega t\right)\sin x = 0 \tag{16}$$

where g is gravitational acceleration, L is the length of the pendulum support and amplitude $\frac{A\omega^2}{L} = \epsilon$. The general form of parametric excitation is defined by the term $\sin x$, where x is the angle of deflection. In order to drive the system by a smooth continuous sinusoidal wave (Figure 7b), the vertical motion described by $\epsilon\cos\omega t$ is approximated by a piece-wise constant function (Figure 7c). This would practically mean that when $x \approx 0$, the $\sin x$ expands in a Taylor series:

$$\sin x \approx x - \frac{x^3}{3!} + \frac{x^5}{5!} - \frac{x^7}{7!} + ... \tag{17}$$

and when $x \approx \pi$, the term $\sin(x + \pi) = -\sin x$ expands in a Taylor series:

$$-\sin x \approx -x + \frac{x^3}{3!} - \frac{x^5}{5!} + \frac{x^7}{7!} - ... \tag{18}$$

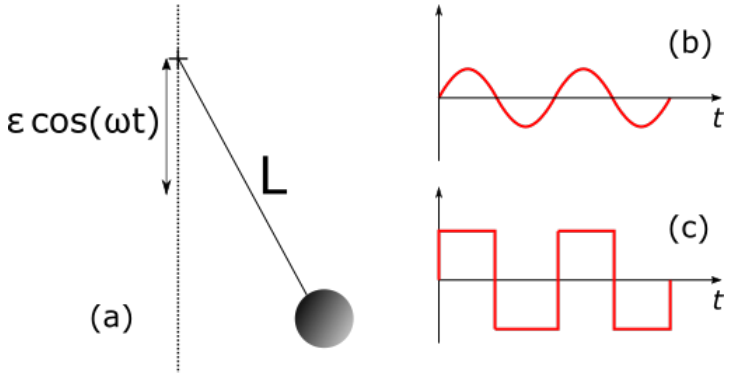

Figure 7: Vertically excited simple pendulum

This linearization (17,18) returns in piece-wise oscillation:

$$\ddot{x} + (\delta + \epsilon \cos \omega t)x = 0 \quad \text{for} \quad 0 < t < T/2$$
$$\ddot{x} + (\delta - \epsilon \cos \omega t)x = 0 \quad \text{for} \quad T/2 < t < T$$

where $\delta = \dfrac{g}{L}$

For the case (ii), it is known that the solution of (15) results in (δ, ϵ)-plane consists of regions of stability (s) and instability (u) bounded by curves on which there is a periodic solution [62], as shown in Figure 8. The unstable zones (u) form "tongues" attached to the δ-axis at $\delta = s^2$, $s = 0, 1, 2, \ldots$. To determine the transition curves between stable and unstable regions numerous methods, including two variable expansion perturbation method [63] and Floquet theory, could be applied.

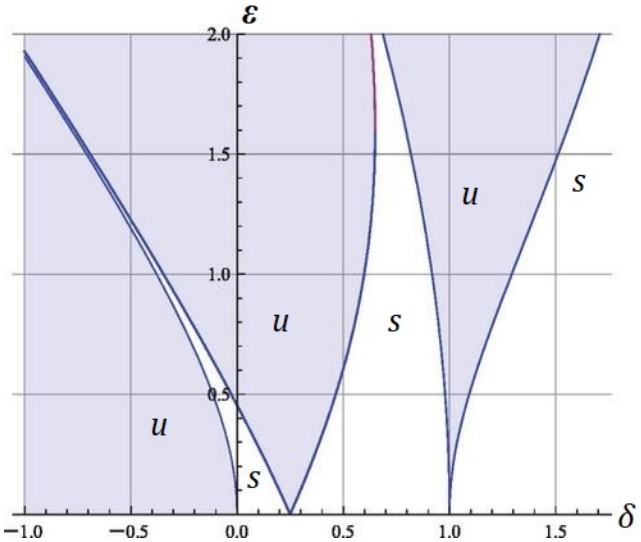

Figure 8: Ince–Strutt diagram of Mathieu equation: s - stable region, u - unstable region
Source: `https://aapt.scitation.org/doi/10.1119/1.5021895`

Damped Mathieu equation

The Mathieu equation describes parametric perturbations in the displacement of the system. The previous case (15) neglected damping effect on the system and reduced the problem to

a broader class of periodic differential equations, termed Hill equation:

$$\ddot{x} + p(t)x = 0 \tag{19}$$

where periodic function $p(t) = \delta + \epsilon \cos \omega t$ and $p(t) = p(t + T)$ for all periods of T.

However, the natural damping exists in all non-linear systems and can be introduced in Mathieu equation:

$$\ddot{x} + b\dot{x} + (s^2 + \alpha + \epsilon \cos \omega t)x = 0 \tag{20}$$

where b, α, ϵ are small and $\delta = s^2 + \alpha$.

In the damped Mathieu equation for a given value of b there is a minimum value of ϵ necessary for instability to occur [61]. The approximate curves for $s = 1, 2, 3$ and $c = 0, 0.2, 0.4, 0.8$ are depicted in Figure 9. The tongue s=1, which for $b = 0$ (solid line) emerge from the δ-axis, for $b > 0$ (dashed line) becomes detached from δ-axis. Note that, if the $b > 0$, the exact curves for different values of s should not cross the δ-axis. This prediction was verified in [61] for a fixed b and varrying δ and ϵ parameters. Due to this condition, the domain of the "tongues" (in Figure 9) artificially restricted. For the detailed solution see [61, 62].

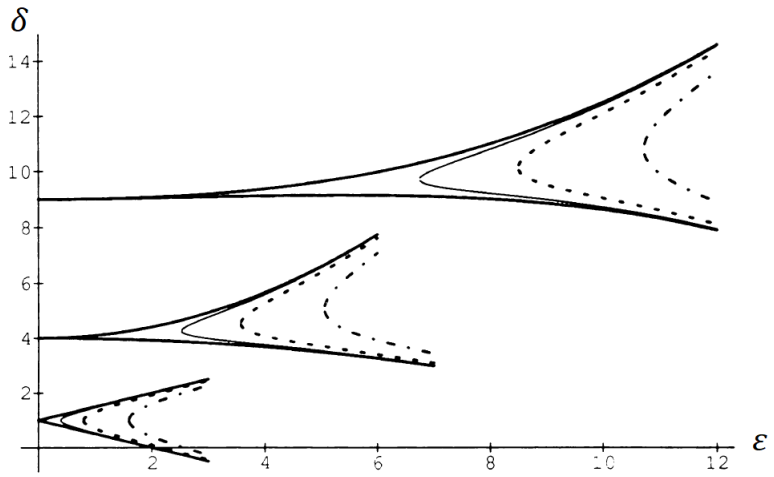

Figure 9: Approximate curves for varying s, b parameters [62]

2.4 Carson−Cambi Equation

The Carson-Cambi equation is another variation of a periodic differential equation, that differs from the Mathieu equation (15) with the time-varying coefficient associated with the second derivative:

$$(1 + \epsilon \cos t)\ddot{x} + px = 0, \quad |\epsilon| < 1 \tag{21}$$

where p and ϵ are the real coefficients.

In the theory of frequency modulation (where $\epsilon \ll 1$), utilizing [64, 65], the solution of the equation (21) is to replace it by Mathieu's equation (15) in a form:

$$\ddot{x} + p(1 - \epsilon \cos t + 0(\epsilon^2))x = 0 \tag{22}$$

for which an extensive literature exists [66]. Another approach is to apply quantitative analysis to determine how "strong" the stability-instability is for given parameters p, ϵ described in [67]. Thus, will result in qualitative (on/off) information. To determine solutions corresponding to specific initial conditions, numerical simulation has to be done. The results have been compared with perturbation analysis [66] and the method proved to be more convenient. However, it also showed that the approach should not be used for $|\epsilon| > 0.4$.

To begin quantitative analysis the term t has to be substituted $t = 2\tau$, where τ has periodicity of π. The Carson-Cambi equation will take a form:

$$\ddot{x} + 4p(1 + \epsilon \cos 2\tau)^{-1} x = 0 \tag{23}$$

where $\ddot{x} = d^2x/d\tau^2$ and $(1 + \epsilon \cos 2\tau)^{-1}$ is an even, periodic function

Note that the stability analysis is independent of the sign of ϵ, such that if we substitute $t = -\tilde{t} + \pi$ and $\epsilon = -\tilde{\epsilon}$, we get

$$(1 + \tilde{\epsilon} \cos \tilde{t})\ddot{x} + px = 0 \tag{24}$$

equation similar to (21) [67].

Introducing the Fourier expansion for even, periodic function

$$\ddot{x} + \frac{4p}{\sqrt{1-\epsilon^2}} \left\{ 1 + 2 \sum_{n=1}^{\infty} \left[\frac{-\epsilon}{1 + \sqrt{1-\epsilon^2}} \right]^n \cos 2n\tau) \right\} x = 0 \tag{25}$$

and replacing $x(\tau) = e^{b\tau} z(\tau)$, the result is

$$\ddot{z} + 2b\dot{z} + \left\{ \left[\frac{4p}{\sqrt{1-\epsilon^2}} + b^2 \right] + 2\frac{4p}{\sqrt{1-\epsilon^2}} \sum_{n=1}^{\infty} \left[\frac{-\epsilon}{1 + \sqrt{1-\epsilon^2}} \right]^n \cos 2n\pi) \right\} z = 0 \tag{26}$$

The quantitative stability analysis of the Hill equation (detailed in [68]) transforms equation (26) to

$$\ddot{z} + 2b\dot{z} + \{a_{2n} + 2q\phi(\tau)\} z = 0 \tag{27}$$

where $\phi(\tau)$ is a periodic function with period π. Therefore, the solution of equation (27), according to [68],

$$\phi(\tau) = \sum_{n=1}^{\infty} a_{2n} \cos 2n\tau, \tag{28}$$

where

$$\begin{aligned} a_{2n} &= \left[\frac{-\epsilon}{1 + \sqrt{1-\epsilon^2}} \right]^n = a_2^n, \\ q &= \frac{4p}{\sqrt{1-\epsilon^2}}, \\ a &= q + b^2 \end{aligned} \tag{29}$$

From the following, the solution of actual parameters can be calculated:

$$\begin{aligned} \epsilon &= a_2[1+\sqrt{1-\epsilon^2}] = \frac{-2a_2}{1+a_2^2} \\ p &= \frac{q}{4}\sqrt{1-\epsilon^2} = \frac{q}{4}\frac{1-a_2^2}{1+a_2^2} \end{aligned} \tag{30}$$

The stability of solutions (29) and (30) can be determined as an eigenvalue problem. Given p and ϵ determine b in stability diagram. The final results must be used in inverse sense, for instance, if b is positive real solutions $x(\tau)$ will be unstable as $z(\tau)$ is periodic and the value b shows how "strong" the exponential factor is. If b is purely imaginary, the solution $x(\tau)$ will be periodic, i.e. stable. The detailed stability analysis will be discussed in the Chapter 3.

3 Stability of solutions

This chapter is dedicated to the the fundamental characteristics of stability of the system and possible ways to solve it, such as the eigenvalues, Poincaré Diagram, and Floquet theory. The term stability usually refers to the stable and unstable solutions of differential equations; and trajectories of dynamical systems. A stable solution is an important, and often desirable property of a dynamic body subjected to small, unpredictable disturbances. Even tiny perturbations could eventually cause a large alternation from the equilibrium if the system is unstable. On the other hand, this significant deviation can be used to enhance the power output. Whereas in the stable systems, the oscillations have initially high amplitude after some period of time settle at the low, close to 0, values, in the unstable systems, the oscillations have an exponential increase in amplitude. In other words, for the unstable system, the absolute velocity and displacement values are increasing in time and since the power is directly proportional to the velocity, it increases alongside.

In mechanics, the stability of the system can be determined using the system's potential energy function. For a single degree of freedom system, the second derivative test can be used in the following way:

$$\frac{\partial^2 V}{\partial q^2} = \lambda, \text{ where } \begin{cases} \lambda < 0 & \text{for stable solutions} \\ \lambda > 0 & \text{for unstable solutions} \end{cases}$$

The V is the static equation of motion and q is the system's degree of freedom (DOF). If the $\lambda = 0$ or solution does not exist, the system is in neutral equilibrium and the higher order derivatives must be examined.

In Figure 10 the stability is described in terms of a ball that is either on the hill or in the valley. The unstable system has a positive feedback, like when the ball stands on top of the hill. Although it is stable at the moment, even small perturbation will make gravitational forces act in the same direction with the ball movement (positive feedback) to push the ball farther from its undisturbed position. On the other hand, when the ball is in a valley, the system is stable and has a negative feedback. Therefore, the gravitational forces will act in the direction opposite to the ball displacement to return the ball to its undisturbed position. When the ball is in the saddle point, it will nearly remain in equilibrium if displaced a small amount, in other words, it is asymptotically stable. The ball approaches equilibrium at some point in time, and losses it at another, the feedback will depend on initial conditions.

There are various methods to solve the stability problem. A general method would involve *Lyapunov functions*, where the point near equilibrium is under study. If the point starts out near an equilibrium point and remains there forever the system is Lyapunov stable. However, there is no general technique for constructing Lyapunov functions, the specific case has to be studied independently. Locating Lyapunov functions is a complex question, therefore it is more favorable to reduce the task to a well-studied problem involving eigenvalues of matrices.

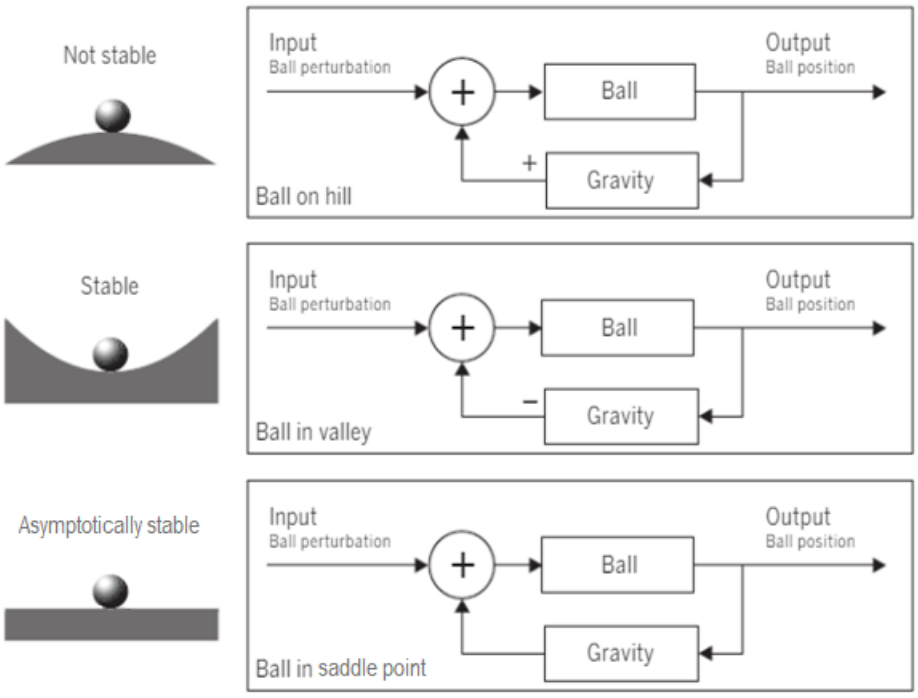

Figure 10: Potential energy stability test [69]

3.1 Stability and eigenvalues

Eigenvector and eigenvalue are the specific characteristics of a square matrix originally used to study principal axes of the rotational motion of rigid bodies. They are fundamental in the linear transformation analysis as well as prominently used in a wide range of areas of linear dynamics [70]. The study of eigenvectors and eigenvalues of the matrix is called spectral analysis.

An eigenvector of an $n \times n$ matrix M is a nonzero vector $\boldsymbol{\rho}$ in a scalar field R^n, that

$$M\boldsymbol{\rho} = \lambda\boldsymbol{\rho} \tag{31}$$

where λ is an eigenvalue. An eigenvalue of M is any scalar such that the equation 31 has a nontrivial solution, but unlike eigenvectors, eigenvalues may equal to zero. Eigenvertors get streched, shrunk or reflected upon matrix multiplication. When the linear transformation T is applied, the eigenvector of T gets scaled by an eigenvalue λ, however the direction of $\boldsymbol{\rho}$ remains the same. This condition can be written as the equation:

$$T(\boldsymbol{\rho}) = \lambda\boldsymbol{\rho}.$$

In order to find solutions for eigenvector and corresponding eigenvalue, the equation 31 will be written in form:

$$(M - \lambda I)\boldsymbol{\rho} = \mathbf{0}, \tag{32}$$

where I is the $n \times n$ identity matrix and $\boldsymbol{\rho} \neq \mathbf{0}$. Therefore, the matrix $(M - \lambda I)$ cannot have an inverse and the equation, where the determinant of matrix:

$$det(M - \lambda I) = 0 \tag{33}$$

called *characteristic equation*. The eigenvalues are reducing a 2-dimensional problem to a couple of 1-dimensional problems, that each set of solutions is bounded to 1 DOF. The number of solutions of eigenvalues coincide with the size of the matrix, in this case $\lambda = \{\lambda_1, \lambda_2, \lambda_3 ... \lambda_n\}$. Since M is a real matrix, its eigenvalues and corresponding eigenvectors can be real numbers or a complex conjugate pairs. For the real λ, the solution is *stable* if all associated $\lambda < 0$; and *unstable* if all associated $\lambda > 0$. For the complex λ, the stability is characterized by the real part of eigenvalue $Re(\lambda) < 0$, for *stable*; and $Re(\lambda) > 0$ for *unstable* solutions.

As was mentioned earlier, the principles of eigenvectors and eigenvalues frequently utilized in stability theory. For instance, a dynamical system described by ordinary differential equations, $\dot{\boldsymbol{x}} = \boldsymbol{f}(\boldsymbol{x}, t)$, consist of the real state vector $\boldsymbol{x}$ and differentiated with respect to time t. The real vector-function $\mathbf{f}$ depends on the variables and initial conditions $\boldsymbol{x}(t_0) = \boldsymbol{x_0}$, providing existence and uniqueness of solutions on semi-infinite interval of time $t \geq t_0$. If the vector-function $\mathbf{f}$ does not depend on time explicitly, the system is *autonomous*, otherwise, *non-autonomous* [71]. The system with two parameter (x_1 and x_2), such as:

$$\dot{x}_1 = ax_1 + bx_2$$
$$\dot{x}_2 = cx_1 + dx_2$$

where a, b, c, d are the coefficients, can be written in a form:

$$\dot{\boldsymbol{x}} = A\boldsymbol{x}, \tag{34}$$

where A is a state-transition matrix:

$$A = \begin{bmatrix} a & b \\ c & d \end{bmatrix}$$

The state transition matrix is used to obtain the generalized solution of linear dynamical systems. The product of A with the state vector $\boldsymbol{x}$ at initial time t_0 gives $\boldsymbol{x}$ at period of time t. The characteristic equation for a state matrix A (applying equation 33) is:

$$\lambda^2 - (a + d)\lambda + (ad - bc) = 0 \tag{35}$$

and the solution for the eigenvalues will be:

$$\lambda_{1,2} = \frac{(a + d) \pm \sqrt{(a + d)^2 - 4(ad - bc)}}{2} \tag{36}$$

if $(a + d)^2 \geq 4(ad - bc)$, the associated eigenvalues are real numbers, otherwise it will be complex numbers.

3.2 Stability and trajectories

A path that system (with mass) in motion takes through space as a function of time is called trajectory, and by Hamilton mechanics is defined by position and momentum vectors [72]. The motion of a particle can be described by the second order ODE:

$$m\ddot{\boldsymbol{x}}(t) = -\nabla V(\boldsymbol{x}(t)), \tag{37}$$

where position vector $\boldsymbol{x} = [x, y, z]$ and ∇V is the potential gradient[11]. Trajectories of the dynamical system can be geometrically represented in a phase portrait, that each set of initial conditions associated with a different curve/point. In this case, the eigenvalues have the same meaning as the slope of a line in phase portrait.

The Poincaré Diagram (Figure 11) illustrates the stability of solutions of trajectories of a body under small perturbations of initial conditions. A relationship between determinant and trace of the any matrix and its eigenvalues:

$$det(A) = \prod_{i=1}^{n} \lambda_i \tag{38}$$

$$Tr(A) = \sum_{i=1}^{n} \lambda_i \tag{39}$$

can be used to describe the classifications of phase portraits in the $(detA, TrA)$-plane. The x-axis represents the determinant of matrix $(detA)$ and the y-axis is the matrix trace (TrA), the matrix discriminant is $\Delta = (TrA)^2 - 4detA$.

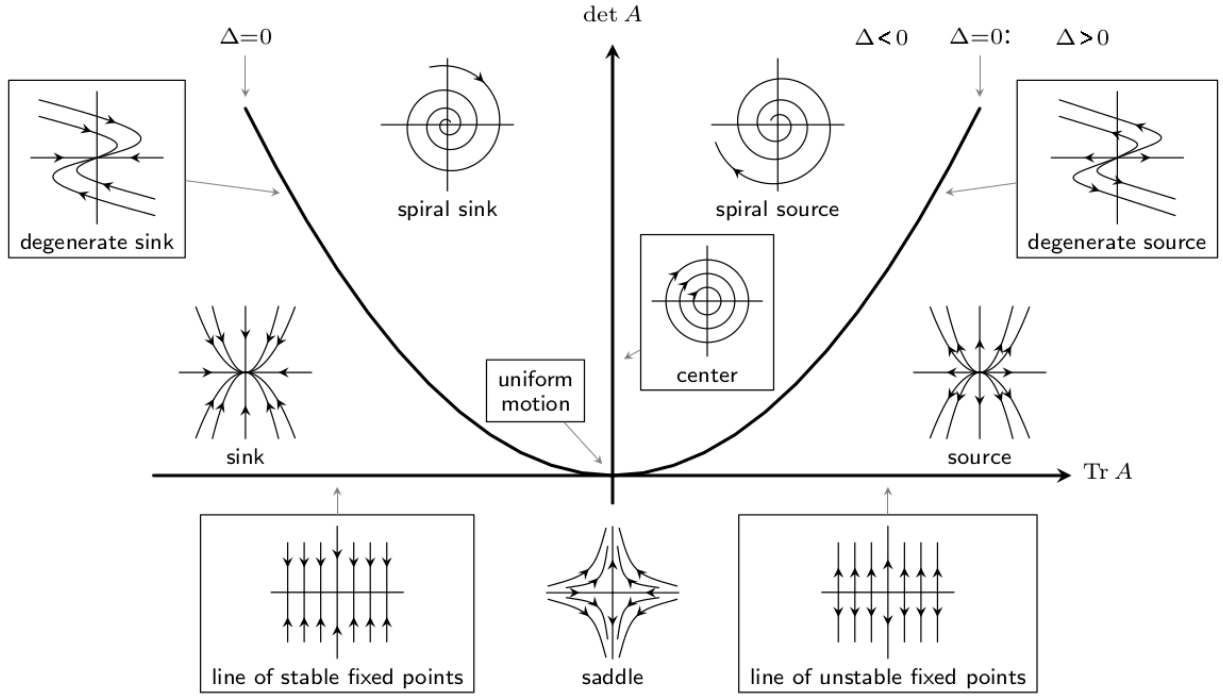

Figure 11: Poincaré Diagram: Classification of Phase Portraits in the $(detA, TrA)$-plane
Source: Gimp, Stability Diagram, 4/2/2018, Freesodas

Different phase portraits depicted in Figure 11 can be categorized in: generic cases, borderline cases and other special case. The generic cases are the following:

- if $det(A) < 0 \quad \Rightarrow \quad$ *saddle point*
- if $det(A) > 0$ and $\Delta > 0 \quad \Rightarrow \quad$ *spiral sink/source*
- if $det(A) > 0$ and $\Delta < 0 \quad \Rightarrow \quad$ *nodal sink/source*

[11] local change rate of potential due to displacement

The trajectories of *unstable* solution move out ("source") to ∞ for $t \to \infty$ and approach 0 for $t \to -\infty$, the trace would be positive ($Tr > 0$), whilst *stable* solution's trajectories approach ("sink") 0 for $t \to \infty$ and move out to ∞ for $t \to -\infty$ and the trace would be negative ($Tr < 0$). The borderline cases consist of the following:

- if $Tr(A)$=0 and $det(A) > 0$ $\Rightarrow$ *center*
- if $Tr(A) \neq 0$ and $det(A) = 0$ $\Rightarrow$ *line of fixed points stable/unstable*
- if $det(A)$>0 and $\Delta = 0$ $\Rightarrow$ *degenerate sink/source*

When the matrix $A = \lambda$ and $\lambda \neq 0$ it is the other special case called *stable/unstable star*, depend on whether $\lambda < 0$ or $\lambda > 0$.

As $t \to \pm\infty$, each trajectory exhibits one of only four types of behavior. The useful tool to understand the long term behavior of a dynamical system is a limit set. Limit set is the state that dynamical system reaches after an infinite amount of time has passed, by either going forward or backwards in time [73]. In the [73], four different types of stability of a limit sets are distinguished: *stable but not asymptotically stable, asymptotically stable, unstable* and *non-stable*. The limit set L is stable if all nearby trajectories stay nearby, and asymptotically stable if all nearby trajectories are attracted. On contrary, if all nearby trajectories (except trajectories in L) are repelled, the limit set L is unstable. Nevertheless, if at least one nearby trajectory is attracted, and if at least one nearby trajectory is repelled, the limit set L is non-stable. All the pairings of stability types are mutually exclusive, apart from the asymptotically stable limit set which is also stable. The "non-stable" definition is used to consider reverse-time dynamics of the system. An unstable limit set is asymptotically stable in reverse time, however, non-stable limit set remains non-stable in reverse time.

Poincaré Maps

The Poincaré map, also known as the first recurrence map, is one of the techniques to analyze the continuous dynamical system. From [71], a periodic system described by a nonlinear system of ODE:

$$\dot{\boldsymbol{x}} = \boldsymbol{f}(\boldsymbol{x}, t) \tag{40}$$

where $\mathbf{x}$ is a real vector of n dimension, and $\boldsymbol{f}(\boldsymbol{x}, t)$ is a periodic function of time t with a period $T > 0$, that is $\boldsymbol{f}(\boldsymbol{x}, t + T)$ for any $\mathbf{x}$ and t. A solution of this system is *periodic* if

$$\boldsymbol{x}(t) = \boldsymbol{x}(t + T) \tag{41}$$

Assume that $\boldsymbol{f}(\boldsymbol{x}, t)$ is a smooth function of $\mathbf{x}$ and continuous function of t. Instead of the nth-order continuous-time system[12], such as $\dot{x} = Ax$, Poincaré map presents the $(n-1)$th-order discrete-time system[13], such as $x(n+1) = Ax(n)$. This order reduction and the fact that it acts as a bridge between continuous- and discrete-time systems makes Poincaré map convenient instrument in the analysis of stability [74]. To construct a Poincaré map, one has to trace the state of the system at p_n through the flow map φ over period of T to the next

[12] has an infinite number of points between any two points in time

[13] the values of the variables are occurring as the distinct, separate points in time

mapping point p_{n+1}:

$$p_{n+1} = \varphi(p_n) \tag{42}$$

Any two Poincaré Maps for a periodic orbit are conjugate to each other. For practical problems, Poincaré Map is usually conducted using numerical simulation, where the Poincaré cut/section has to be well-defined by initial conditions. The behavior exhibited on the map can be whether:

- *stable*, if the periodic solution $p_{n+1} = p_n$, or
- *unstable*, if the periodic solution $p_{n+1} \neq p_n$, hence $|p_n - p_{n+1}| > |p_{n+1} - p_n|$

The principles of Poincaré map are used to identify stability regions in Floquet theory. The practicality of the solutions comes from the fact that instead of looking at the entire dynamical trajectory of the system, we are going to look at the "map" from one period to the next, as shown in Figure 12:

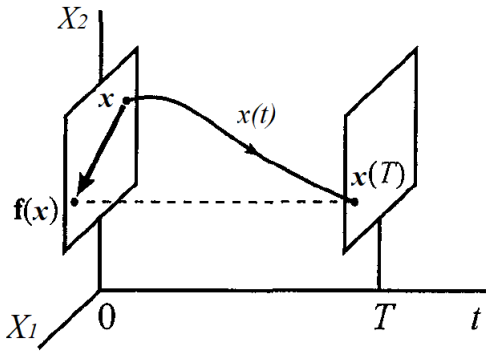

Figure 12: Poincaré map of a periodic system [71]

3.3 Floquet theory

Floquet theory, first introduced by Gaston Floquet in [75], is the study of the stability of linear periodic systems in continuous time (equation 40,41). To solve the Floquet theory, we are going to follow Grimshaw [76] along with Seyranian and Mailybaev [71]. Let consider a linear periodic system of ordinary differential equations:

$$\dot{\boldsymbol{x}} = A(t)\boldsymbol{x} \tag{43}$$

where $\mathbf{x}$ is an n-dimensional vector and $A(t)$ is $n \times n$ matrix which entries are continuous or piecewise continuous functions on $(-\infty, \infty)$. Assume that the equation (43) is going to have n linearly independent solutions $x_1(t), x_2(t), ..., x_n(t)$ that satisfy the initial conditions

$$x_i(0) = e_i, \quad i = 1, 2, ..., n \tag{44}$$

where e_i is the ith column of the $n \times n$ identity matrix I and the solutions satisfying the initial conditions: $\boldsymbol{x}(0) = \boldsymbol{x_0} = (x_{01}, x_{02}, ..., x_{0n})$. Then, solution of the equation (43) satisfying the initial condition x_0:

$$\boldsymbol{x} = \sum_{i}^{n} x_{0i}\boldsymbol{x}_i(t) \tag{45}$$

where $\boldsymbol{x}_i(t)$ are the vector functions[14] with the period of T. The vector $\boldsymbol{x}_i(t)$ can be written as columns of the $n \times n$ real matrix $X(t) = [x_1(t), ...x_n(t)]$, hence:

$$\boldsymbol{x}(t) = X(t)\boldsymbol{x_0} \tag{46}$$

The matrix $X(t)$ satisfies the equation

$$\dot{\boldsymbol{x}} = A(t)\boldsymbol{x}$$

with initial condition

$$X(0) = I \tag{47}$$

and is called the *principal fundamental matrix*. Note that the principal matrix $A(t)$ with period T that defines the state of the stability of solutions, is also periodic with period kT for any integer k, hence $A(t + kT) = A(t)$ for all t. Then, according to [77]:

$$X(t + T) = X(t)B \tag{48}$$

where $B = X(T)$ is a non-singular constant matrix; from induction:

$$X(t + kT) = X(t)B^k \tag{49}$$

Moreover, using Wronskian theorem:

$$detB = exp\{\int_0^T TrA(s)\, ds\} \tag{50}$$

Although, the $A(t)$ has periodically-varying parameters, the solutions are typically non-periodic and rarely found in a closed-form [76]. If equation (48) is true for all t, the constant matrix B can be expressed in terms of fundamental matrix at $t = 0$:

$$B = X^{-1}(0)X(T) \tag{51}$$

and if $X(t)$ is chosen to be principal fundamental matrix, so that $X(0) = I$, and then:

$$B = X(T) \tag{52}$$

Here matrix $X(t)$ taken to the period $t = T$ is called Floquet matrix or monodromy matrix[15], and the matrix operator B represents the Poincaré map $p_{n+1} = \varphi(p_n)$ for periodic system.

Let's consider the eigenvalue problem for Floquet matrix

$$B\boldsymbol{\rho} = \lambda\boldsymbol{\rho} \tag{53}$$

where ρ is an eigenvector and λ is an eigenvalue. Since columns of the B are linearly independent ($detB \neq 0$), the eigenvalues $\lambda \neq 0$. Then the equation (53) yields a particular solution of the discrete dynamical system defined by Floquet matrix:

$$\tilde{\boldsymbol{x}}(kT) = \boldsymbol{B}^k\boldsymbol{\rho} = \lambda^k\boldsymbol{\rho} \tag{54}$$

[14] the domain is a subset of the real numbers and the range is a vector

[15] Monodromy is the transformation of an object when enclosing it along a nontrivial closed path; the fundamental meaning of monodromy comes from "running round singly".

After each period, the solution (54)is multiplied by Floquet multiplier λ. The Floquet multipliers are the eigenvalues of a monodromy matrix B (defined by equation (48) or(51)) that provide period-to-period increase/decrease of the perturbations:

$$\rho_i = e^{\lambda_i T}, \quad i = 1, 2, ..., n \tag{55}$$

where ρ_i is the eigenvector of the matrix, called Floquet exponent, determines the long-term behavior of the system. While Floquet exponent has a unit of time^{-1} and Floquet multiplier is a dimensionless number, both provide the growth rate of different perturbations averaged over a cycle [78]. If the $|\lambda|>1$, the norm of solution (54) exponentially increase with increasing term k, whereas the $|\lambda|<1$, causes the norm to decrease with increasing term k.

The equation (54) describes discrete system that has l linearly independent solutions, and according to Jordanian chain[16]:

$$\begin{aligned}
\tilde{x}_1(kT) =& \boldsymbol{B}^k \boldsymbol{\rho_0} = \lambda^k \boldsymbol{\rho_0} \\
\tilde{x}_2(kT) =& \boldsymbol{B}^k \boldsymbol{\rho_1} = \lambda^k \boldsymbol{\rho_1} + k\mu^{k-1} \boldsymbol{\rho_0} \\
& \vdots \\
\tilde{x}_l(kT) =& \boldsymbol{B}^k \boldsymbol{\rho_{l-1}} = \sum_{i=0}^{min(k,l-1)} C_k^i \lambda^{k-i} \rho_{l-i-1}, \quad C_k^i = \frac{k!}{i!(k-i)!}, \quad \text{for } k = 0, 2, 3...
\end{aligned} \tag{56}$$

The general solution of discrete system defined by Floquet matrix can be contracted taking a linear combination of solutions (54) and (56) for all the multipliers λ and corresponding Jordanian chains. As the result, the following criterion of stability for discrete system are obtained:

- Linear periodic system (43) is *asymptotically stable*, hence, $(||\boldsymbol{x}(t)|| \to \infty$ as $t \to \infty$ for all solutions $\dot{\boldsymbol{x}}(t)$ if and only if $|\lambda| < 1$ for all Floquet multipliers.
- Linear periodic system (43) is *stable*, hence, all solutions $\dot{\boldsymbol{x}}(t)$ are bounded as $t \to +\infty$ if and only if $|\lambda| \leq 1$ for all Floquet multipliers with some multipliers having the unit absolute value $|\lambda| = 1$
- Linear periodic system (43) is *unstable*, hence, there is a solutions $\dot{\boldsymbol{x}}(t)$ that is unbounded as $t \to +\infty$, if and only if there is a Floquet multiplier $|\lambda| > 1$

According to [71], if linearized periodic system (43) is *asymptotically stable* ($|\lambda| < 1$), then the periodic solution $\tilde{\boldsymbol{x}}(t)$ of **nonlinear periodic system** is *asymptotically stable*; and if linearized periodic system (43) is *unstable* ($|\lambda| > 1$), then the periodic solution $\tilde{\boldsymbol{x}}(t)$ of **nonlinear periodic system** is *unstable*. The case when $|\lambda| \leq 1$ for all the multipliers with some multipliers lying on the unit circle $|\lambda| = 1$, the stability property can be affected by non-linears, therefore stable solutions of linear system does not necessarily lead to the same property for the non-linears.

[16] a number of linearly independent eigenvectors is less than the algebraic multiplicity

4 Test case

The WEC is a mechanical device that harvests energy stored in an ocean wave. The extracting power rate regimented by the PTO technology. For direct mechanical drive PTO systems, the primary function is to translate the mechanical energy of an oscillating body subjected to waves into electricity [79]. During the operation, an oscillating body will change its mass by capturing and ejecting water from its floats.

Before any construction of an experimental device, the suggested water intake system has to be simulated numerically to discover its performance potential. To show the efficiency of the mass modulation schemes, the simplest possible model have to be developed and analyzed. Assuming a continuous dynamical approach, a single DOF mass-spring-damper with a harmonically varying mass model will be used to approximate the perturbation in the system. The behavior of this system can be described by the second-order differential equation, similar to the Mathieu equation (15), but with a periodic coefficient in inertia second derivative specified by the Carson-Cambi equation (21).

The model has arbitrary parameters, such as initial mass and spring coefficient, and a set of values for parameters such as damping and modulation coefficient. The optimization requires using numerical integration for the whole range of values and tuning the model up to most beneficial, yet practical use. The evaluation will be conducted in terms of power output and consists of 3 steps:

(i) A notionally common model has to be detected and the performance of such model carefully analyzed. This model will serve as a reference for the future power performance estimations.

(ii) The dynamics of the parametrically excited model have to be investigated. The conditions for the parametric resonance have to detected and reached. Additionally, the limits of the excitation have to be discussed and a realistic threshold settled.

(iii) A further analysis of the system has to be made in order to determine its long-term behavior. From the analysis of the non-linear dynamics, the Floquet theory will be used to identify the possible regions of instability and the results will be verified by numerical integration of the system.

4.1 Model set-up

The developed model of WEC will be similar to a linear oscillator and consists of single DOF mass-spring-damper system, shown in Figure 13. According to the works of Salter and Chiang [80,81], a PTO system could be simulated with a damping element, respectively the measured power is the one contained in the damping term. The effect of the incident waves is modeled by an external harmonic motion. The aim of the model is to investigate how the power collected from the PTO varies with time-dependent mass modulation.

In Figure 13 we can see that the mass of the system varies with time t, and oscillated by externally applied periodic force F_{ex} (eq. (7)):

$$F_{ex}(t) = F_0 \sin(\omega t),$$

and the internal time-varying parameter $M(t)$:

$$M(t) = M_0 \sin(\omega_f t) \tag{57}$$

where ω_f is a mass modulation frequency. The amplitude of oscillations M_0 is defined by the mass of the system m_0 and the mass modulation coefficient μ:

$$M_0 = \mu m_0 \tag{58}$$

essentially, means that the μ is a dimensionless number acting as a percentage of original mass m_0.

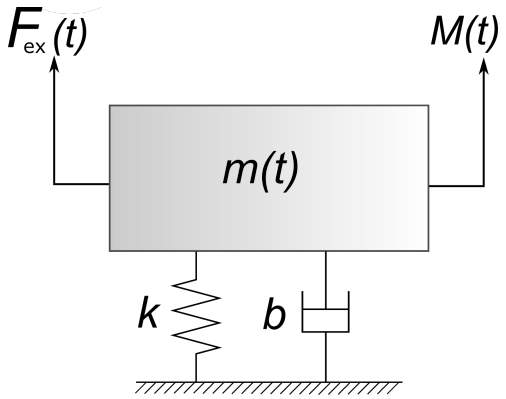

Figure 13: Schematic for a single DOF model of WEC

Taking all of the above, the governing equation for the mathematical model of the oscillating body:

$$m(t)\ddot{x} + b\dot{x} + kx = F_{ex} \tag{59}$$

where damping coefficient b defines PTO rate, spring coefficient k is related to the natural frequency, and $m(t)$ is a mass of the system. The periodic parameter $m(t)$ consists of the original mass of the system m_0 and the time-varying term $M(t)$:

$$m(t) = m_0 + M(t) = m_0 + \mu m_0 \sin(\omega_f t) \tag{60}$$

and the period of this parametrically excited system:

$$T_f = \frac{2\pi}{\omega_f} \tag{61}$$

The power will be measured at every time-step by damping coefficient b and associated velocity $\dot{x}$:

$$P = b\dot{x}^2 \tag{62}$$

and then averaged:

$$\overline{P} = \frac{1}{n}\sum_{i=1}^{n} b_n \dot{x}_n^2 \tag{63}$$

The averaging happens over second half of the simulation[17] to allow initial transients to decay and any resonance to develop.

Model parameters

The system (59) has a simulation running time $t = 100$ seconds and an arbitrary chosen parameters listed in Table 1. The model is also considering modifications in parameters listed in Table 2, by varying them throughout an array of different simulations, in order to investigate its effect on the power output and optimize the system.

Table 1: Invariable parameters for the given simulation model

Notation	Name	Value	Unit
ω	driving frequency	0.7	rad/s
F_0	amplitude of external forcing	1	N
k	spring constant	1	N/m
m_0	initial mass of the system	1	kg

Table 2: The set of parameters varied across different simulations

Notation	Name	Range	Unit
μ	mass modulation coefficient	0.01...0.3	-
ω_f	mass modulation frequency	0.1...3	rad/s
b	damping coefficient	0.001...1	Ns/m

Model normalization

To determine the efficacy of the parametric resonance in the model a normalization has to be made. Normalization is adjusting measured values on the mass modulated model to a notionally common model. A simulation of an additional model that has constant mass ($m = m_0$) is made as a baseline case, therefore the results from the time-varying mass cases are normalized against this baseline model. The governing equation of model:

$$m\ddot{x} + b\dot{x} + kx = F_0 \sin(\omega t) \tag{64}$$

This model is used to show power factor - correlation between power of system with and without mass modulation:

$$n = \frac{\overline{P}_m}{\overline{P}_c} \tag{65}$$

where $\overline{P}_m$ is averaged power of model with periodic mass and $\overline{P}_c$ is averaged power of model with constant mass.

[17] e.g. for the 100 second simulation, the values after 50 seconds passed will be taken into account

In some cases, normalization will refer to more sophisticated adjustments with the intention to bring entire values into alignment. To be specific, a comparison to the model at resonance. As was already mentioned, conventional WEC is designed that the natural frequency of such device resonates with incident wave frequency. The model will have same equation (64) as "common model". This model will be tuned with an optimum damping coefficient to extract the maximum possible power. The mass of the model will be constant.

4.2 Stability analysis with Floquet theory

The equation under study is the equation of the system (59) without periodic forcing ($F_{ex} = 0$):

$$m(t)\ddot{x} + b\dot{x} + kx = 0 \tag{66}$$

The oscillations due to forcing F_{ex} are neglected in order to transform the problem to the field of linear dynamics, where the solutions of stability are defined. However, in the futher analysis the effect of external excitation on stability of parametrically excited system will be shown using numerical simulations. The mass of the system $m(t)$ is periodic with time t, such that $m(t+T) = m(t)$ for all t. Note that the T in this case (and further) is the period of parametric excitations, hence

$$T = T_f = \frac{2\pi}{\omega_f} \tag{67}$$

The system's mass can be expressed by constant term m_0, mass modulation ratio μ and mass modulation frequency ω_f:

$$m(t) = m_0(1 + \mu \sin(\omega_f t)) \tag{68}$$

The periodic mass term $m(t)$ classifies equation (66) into Carson-Cambi equation (21). To solve and determine stability regions, the equation has to be transformed into a damped Mathieu equation and then apply Floquet theory.

The damped Mathieu equation (20) is the regrouped equation (66) of the system:

$$\ddot{x} + \frac{b}{m(t)}\dot{x} + \frac{k}{m(t)}x = 0 \tag{69}$$

for simplicity, we are going to write it in a form:

$$\ddot{x} + p_1(t)\dot{x} + p_2(t)x = 0 \tag{70}$$

where the coefficients p_1 and p_2 are periodic, hence $p_1(t) = p_1(t+T)$ and $p_2(t) = p_2(t+T)$. Note that, if $p_1 = 0$ the equation (70) is reduced to the Hill's equation (19).

To utilize the Floquet theory, the equivalent first-order system of equations ($x_1 = u, x_2 = \dot{u}$) has to be formed:

$$\begin{aligned} \dot{x_1} &= x_2 \\ \dot{x_2} &= -p_1(t)x_2 - p_2(t)x_1 \end{aligned} \tag{71}$$

The general form for a linear homogeneous system with periodic coefficient is here 2×2 matrix:

$$\dot{\boldsymbol{x}}(t) = \begin{bmatrix} \dot{x_1} \\ \dot{x_2} \end{bmatrix} = A(t) \begin{bmatrix} x_1 \\ x_2 \end{bmatrix} \tag{72}$$

where state-transition matrix:

$$A(t) = \begin{bmatrix} 0 & 1 \\ -p_2(t) & -p_1(t)x_2 \end{bmatrix} = 0 \tag{73}$$

The fundamental matrix $X(t)$ such that $X(0) = I$ (47):

$$X(0) = \begin{bmatrix} u_1 & u_2 \\ \dot{u}_1 & \dot{u}_2 \end{bmatrix} \tag{74}$$

where u_1 and u_2 are linearly independent solutions such that

$$\begin{aligned} u_1(0) = 1 \quad u_2(0) = 0 \\ \dot{u}_1(0) = 0 \quad \dot{u}_2(0) = 1 \end{aligned} \tag{75}$$

The constant matrix B (51) can be expressed in terms of fundamental matrix by putting $t = 0$, and $X(0) = I$

$$B = \begin{bmatrix} u_1(T) & u_2(T) \\ \dot{u}_1(T) & \dot{u}_2(T) \end{bmatrix} \tag{76}$$

where $u_1\dot{u}_2 - u_2\dot{u}_1 \neq 0$ for all t. The eigenvalue for the Floquet matrix B (equations (32) and (53)):

$$(B - \lambda I)\boldsymbol{\rho} = 0$$

The characteristic multipliers λ are the eigenvalues of B and can be given by equation (33):

$$det(B - \lambda I) = det \begin{pmatrix} u_1(T) - \lambda & u_2(T) \\ \dot{u}_1(T) & \dot{u}_2(T) - \lambda \end{pmatrix} = 0 \tag{77}$$

Since B is 2×2 matrix, we are going to have 2 eigenvalues λ_1 and λ_2 in a form:

$$\lambda_{1,2} = Re(\lambda_{1,2}) + Im(\lambda_{1,2}) \tag{78}$$

The system is discrete and due to the presence of secular terms, there are unbounded solutions growing as a power of time. The stability will be measured within a unit circle, where $|\lambda_{1,2}| > 1$ is for *unstable* solutions and $|\lambda_{1,2}| \leq 1$ is for *stable* or *asymptotically stable* solutions.

4.3 Results and Discussions

A simulations of the model (59), (64), and (66) have been executed using the parameters listed in Tables 1 and 2. The initial conditions for each simulation case $[\dot{x}_0 \quad x_0]$ will be provided and the outcome of the simulations will be presented step by step in the next sections.

(i) Baseline case

To evaluate the performance of parametrically excited WEC, first, the maximum power potential of the model with constant parameters (64) (refer to as common model) has to be detected. In regards, a numerical simulation of power at different damping b and forcing frequency ω values was computed for the initial conditions $[0 \quad 0]$ for the velocity and the displacement of the system. The outcome of the simulation is shown in Figure 14. Note, that by equation (9), (10) the damping coefficient is bound to $b \leq 2$: if the value exceeds 2, the damping ratio ζ gets higher than 1, and the system would show no oscillatory response.

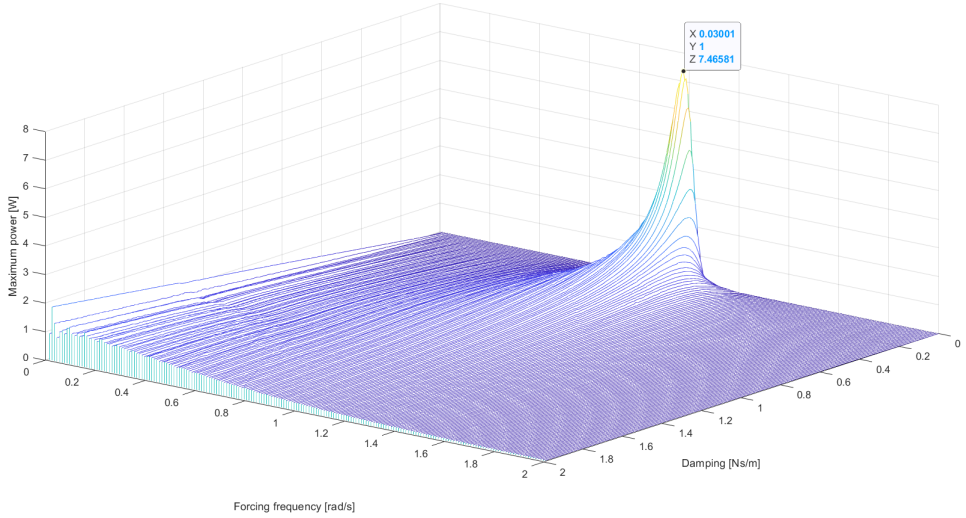

Figure 14: Numerical simulation for the common model (64)

Generally, the power is a product of force and velocity, and in the case of WEC, an oscillating body is stimulated by a dynamic pressure (and, hence, force) of the incoming wave. This force is absorbed by a PTO system that is modeled as a damping element. Altogether, the power distribution depends on damping and velocity, whilst the velocity gets suppressed with a damping coefficient as well. Therefore, as the damping increases the power has a rapid growth until its optimum damping value (b_{opt}) is reached and later, at higher damping ($b > b_{opt}$), the power will only decay (see Appendix 27). In Figure 15, the contour plot of power as a function of forcing frequency and damping is shown. The damping and power have logarithmic scale, so that the nature of the power is more visible. The power has its maximum as the damping gets less than 0.05 and this solution is bounded by forcing frequency $\omega = 1$.

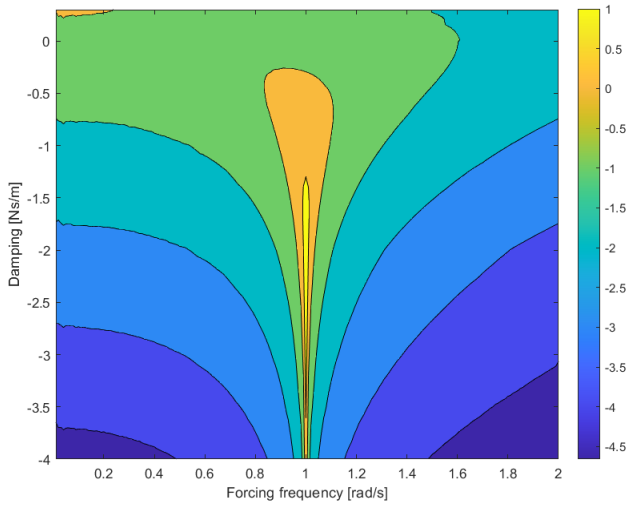

Figure 15: The contour plot of the power at different $\omega - b$ settings for the common model (64). Note that the damping and power values are presented in a log_{10} scale.

From the common model simulations (Figure 14 and 15) running for 100 second a highest power output $\overline{P}_c = 7.47$ happens at the damping $b_{opt} = 0.03$ and forcing frequency $\omega = 1$. Note that the natural frequency of the system $\omega_d = 1$ and from the definition, this substantial transfer of power is caused by the resonance. At the optimum set of parameters (Figure 16.2) the oscillations grow linearly reaching amplitude $d_{max} = 25$ after simulation running for 100 seconds. A detailed view on oscillations of a common model for a different parameter values is shown in Figure 16. Both 16.1, 16.2 and 16.3 are at resonance with natural frequency. However, in 16.1 the power rate is low due to low damping coefficient and the oscillations take more time to build; in 16.3 the damping coefficient is so high, that it suppresses the effect of resonance. Another case, 16.4, is reflecting forced oscillations, but a non-resonant, and has significantly less power output compared to resonant cases.

In Figure 16.1 and 16.2, it is visible that the power output keeps growing, and although, the highest power output $\overline{P}_c = 7.47$, if simulation time is increased the outcome may change. In Figure 17, the same model (64) had a numerical simulation for $t = 1000$ sec and the averaged power for 17.2 settles at a certain value, while in 17.1 the power keeps growing along with amplitude of the oscillations.

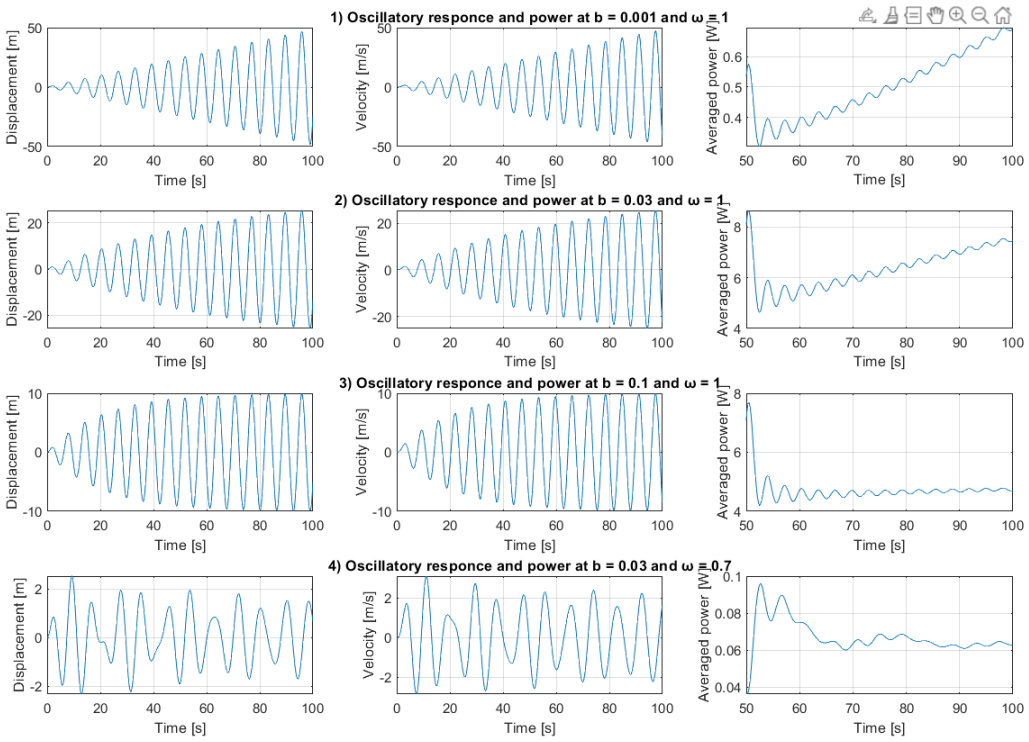

Figure 16: Oscillatory response on the given parameters and averaged power for simulation time $t = 100$ sec.

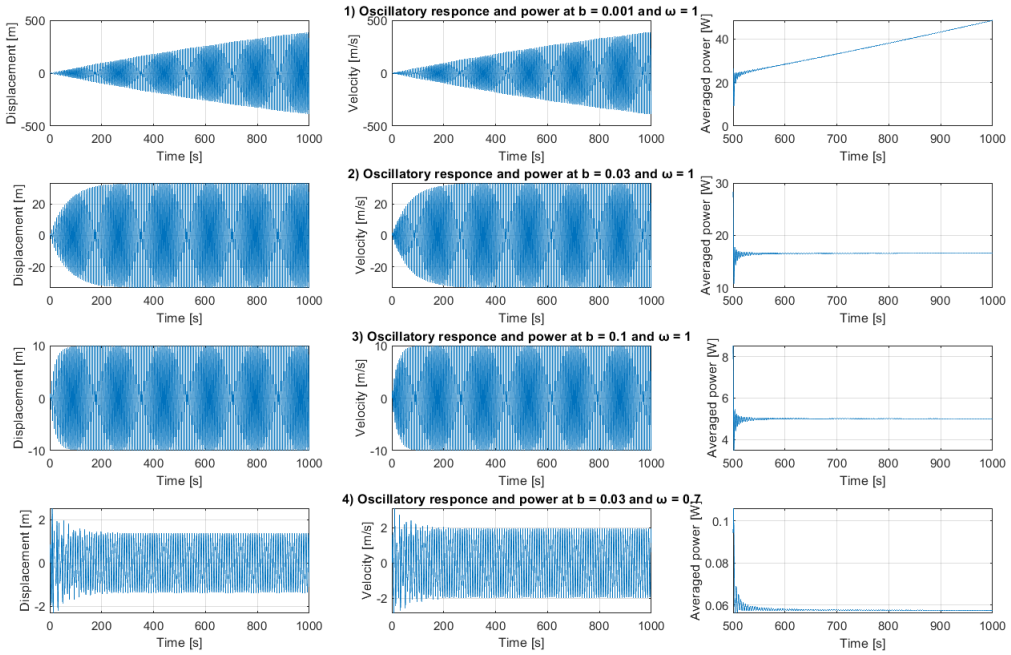

Figure 17: Oscillatory response on the given parameters and averaged power for simulation time $t = 1000$ sec.

(ii) Mass modulation case

The next step is to perform a simulation of model (59) with varying inputs from Table 2. The initial conditions are the same, as for common model: [0 0]. The outcome of simulation is shown as a contour plot of power factor and displacement in Figure 18 and 19. The power (Figure 18) is normalized against no mass modulation model (64) and the displacement d of such model is specified at Figure 19. Although the simulation was running for a wider range of variables, the desired effect is achieved on a certain scale. For instance, the power factor n is significantly higher at the lower damping values and the modulation frequency ω_f twice the natural frequency ω_d. By the definition, this performance is caused by parametric resonance. Nevertheless, at the high damping coefficients, the parametric resonance has no effect, because the energy dissipates at a higher rate than forms, and perturbations decay.

As the mass coefficient μ increases, the power factor n grows along. Note that at some frames (Figure 18) the logarithmic scale $log_{10}(n)$ is used in order to detail the numerical data over a wider range of values. The results show a considerable rise at a very small damping coefficients ($b < 0.1$). The simulation shows that the system could achieve a power factor $n = 10^5$ at $b = 0.001$. This is due to the idealized model[18] of the system. The displacement contour plot (Figure 19) for the same system shows that the amplitude of the oscillations gets to 2500 [m] and continue growing, whilst the common model has a displacement amplitude $d = 2.7$ [m]. In reality, such excessive amplitudes would not be reached due to nonlinear terms bounding the infinite growth, which are not present in the simple linear model examined here. The contour plot for the velocity of the system is provided in the Appendix 28.

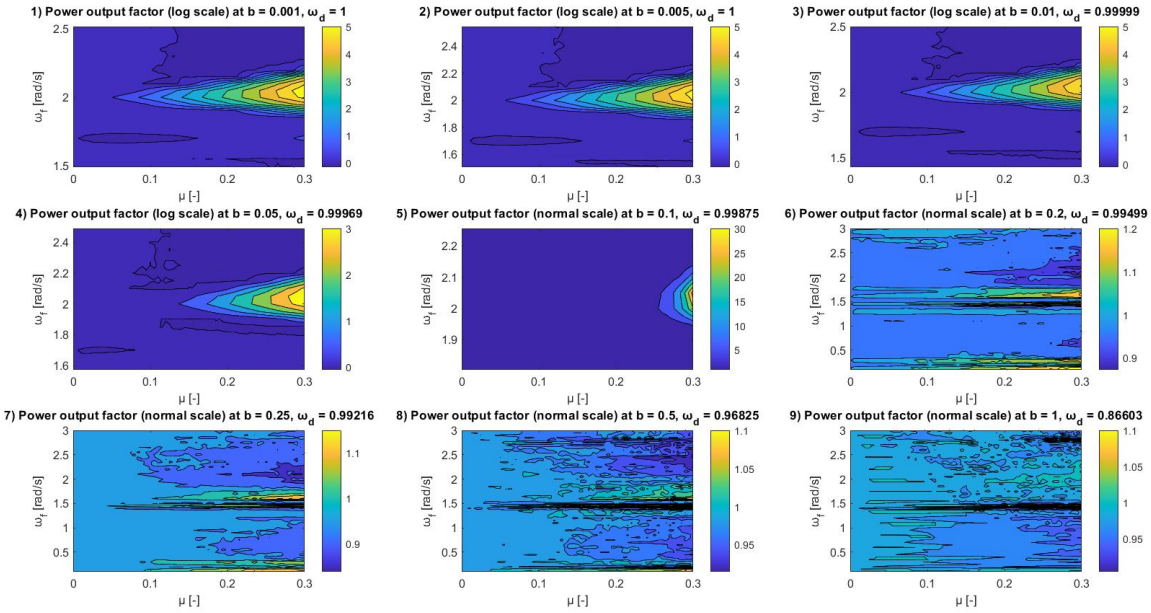

Figure 18: Power output factor at the different damping rate

[18] without any losses

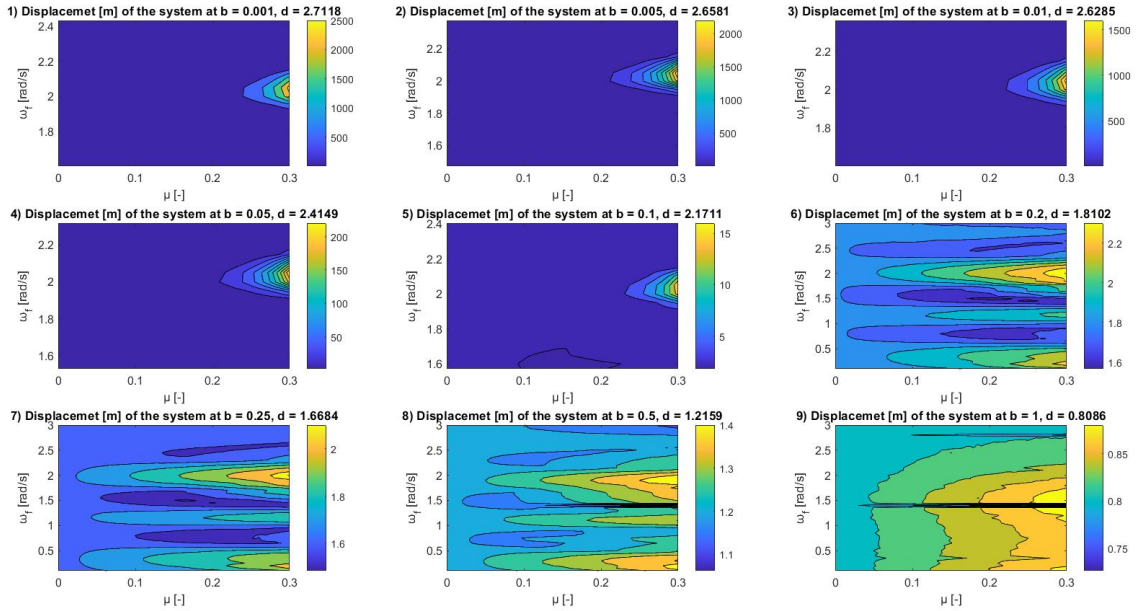

Figure 19: Displacement at the different damping rate

From Figure 18 the highest power output was determined along the modulation frequencies, i.e. the maximum power and associated modulation frequency ω_f. Thereon that modulation frequency, the averaged power distribution $\overline{P}_m$ as a function of the mass modulation coefficient μ is shown in Figure 20. Note that for the $b < 0.2$ the associated (with maximum power) modulation frequency ω_f and the natural frequency ω_d in proportion 2:1, and this does not hold for $b \geq 0.2$ due to high suppression rate.

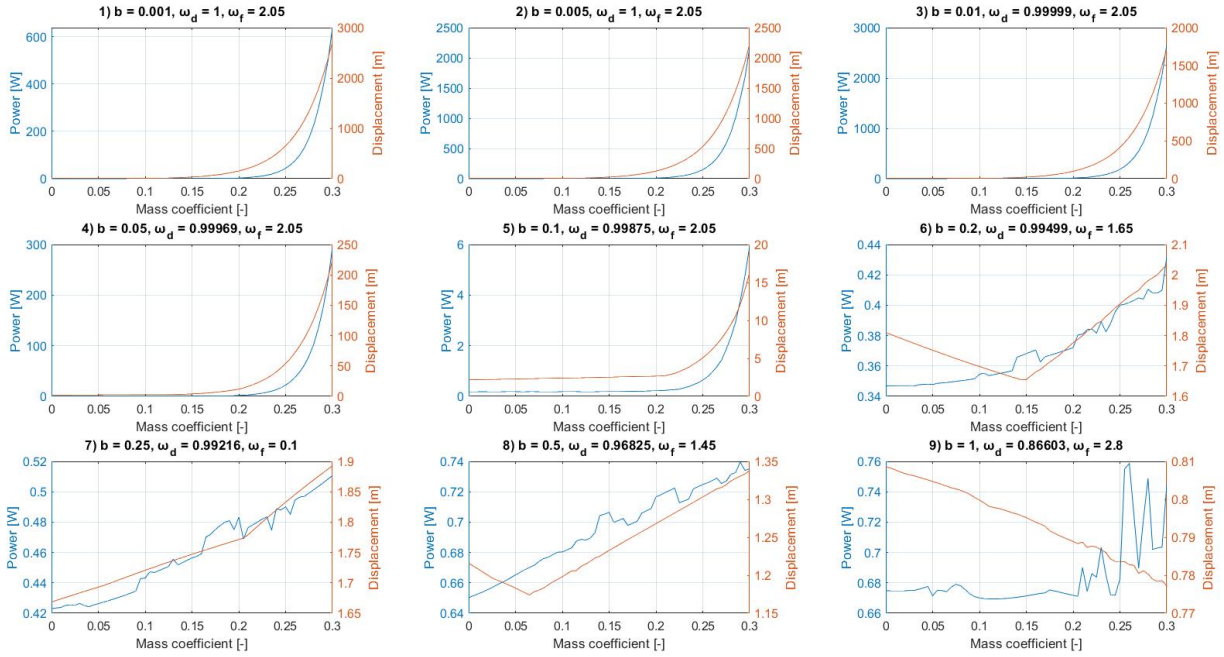

Figure 20: Power and amplitude of oscillations comparison in terms of mass modulation coefficient

Comparing to the common model (Figure 14) with the maximum power $\overline{P}_c = 7.47$, for the mass modulation case close or greater power is detected at $b \leq 0.01$. This decision is guided by the power output presented in Figure 20. The performance of the model at frames 6, 7, 8, 9 are insufficient compared to the common model, therefore, considering using these models is not pragmatic.

In Figure 21 the power distribution at the dedicated damping range ($0.001 < b < 0.01$) and modulation frequency $\omega_f = 2$ is shown. The increase in mass modulation coefficient is leaning towards rising in power. As for the power versus damping coefficient, the distribution is similar to a common model and shown in Appendix 29.

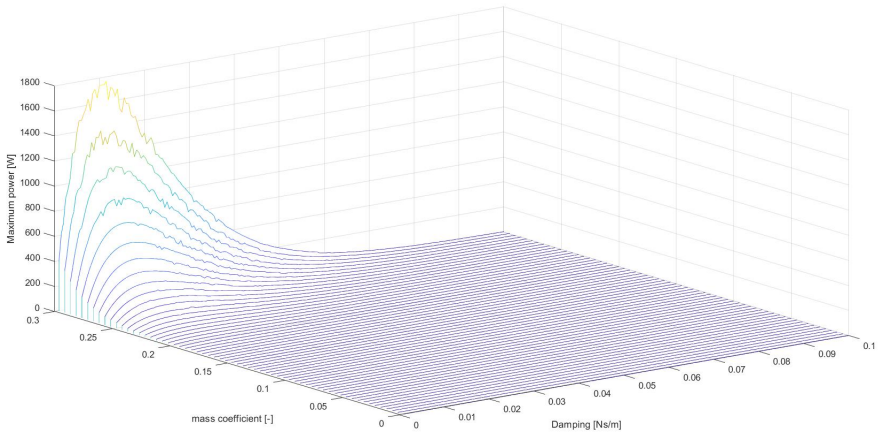

Figure 21: Averaged power distribution at $b = (0.001 : 0.1)$ in terms of mass coefficient

The maximum power has an unrealistic rise after simulation was run for a long time, however at the moderate time the improvements that the system experiences are practical. Let assume a realistic threshold for absolute displacement $d_{max} = 25$; this is a maximum amplitude of the oscillations at the resonance for a common model (see Figure 16 frame 2). Applying a threshold to the system with parametric resonance (Figure 20), and at the $0.005 < b < 0.05$, the wide distribution obtained (Appendix 30). However, the main focus is on the values higher than the maximum power output $\overline{P}_c = 7.47$. This leads to the optimum parameter values (Figure 22 and 23):

- for the mass modulation coefficient $\mu = 0.17$ at the optimum damping $b_{opt} = 0.009$ the maximum averaged power is 32.6% of the common model,
- as the $\mu = 0.2$ and at $b_{opt} = 0.008$ the maximum averaged power is 73.6% of the common model, however
- as the $\mu = 0.25$ and at $b_{opt} = 0.008$ the maximum averaged power is 587% of the common model, and even further
- as the $\mu = 0.3$ and at $b_{opt} = 0.001$ the maximum averaged power is 2193%, which is *over 20 times greater* than the performance of the common model. However, the design complexity and realization cost for such model will be significantly higher (if possible at all) compared to let say $\mu = 0.2$.

The design of the model gets more sophisticated, if it is projected for a larger mass, therefore,

choosing the greatest modulation coefficient may not be the best option.

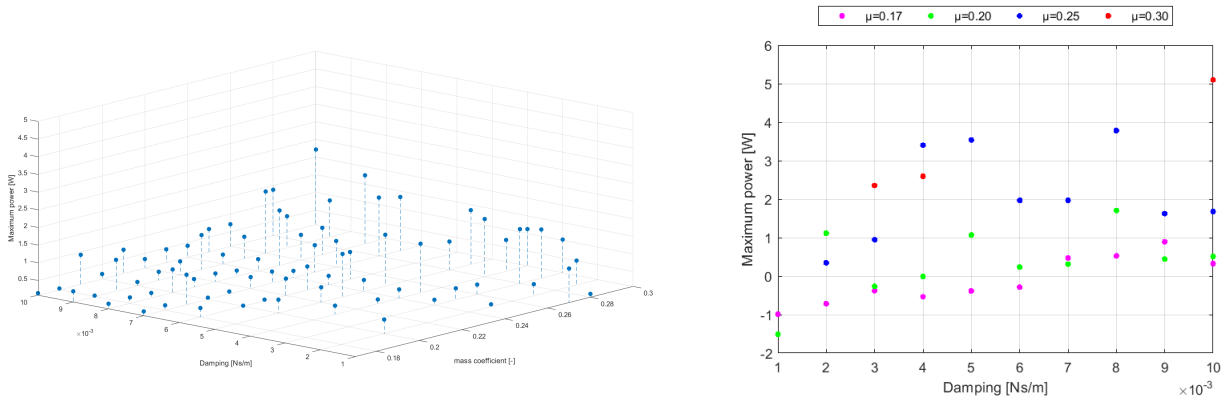

(a) 3D view (b) (damping-power) plane

Figure 22: Scatter of the $\mu - b$ parameter values in terms of power limited by the $\overline{P}_c$. Note that power is in logarithmic (log_{10}) scale.

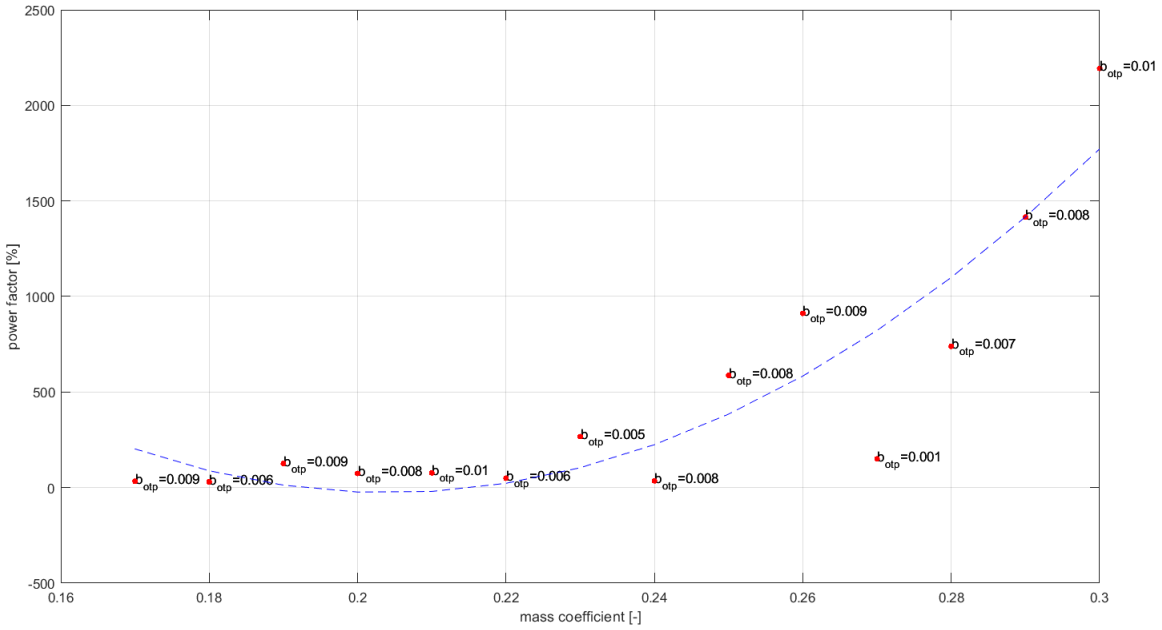

Figure 23: The performance gain in (log_{10}) scale during the increase of mass modulation coefficient.

(iii) Stability analysis

The numerical simulation proved to be a useful tool to analyze the dynamics of the WEC model, however, in order to understand the long-term behavior of the solution, the stability and instability regions have to be detected. The Floquet theory analysis is used to explore the stability from one-period simulation. This will sufficiently decrease the simulation running time and opens an opportunity to introduce other parameters of the non-linear model.

Applying the Floquet theory on model (66) with the modulation frequency ranged in Table 2, and initial conditions in (75), the analysis practices a higher modulation coefficient range $\mu = 0.01...0.5$ in intend to discover the prolonged behavior of the system. Since the phenomenon of parametric resonance causes unstable behavior of the system, the designated instability regions are depicted in red at the Floquet map (Figure 24 and Appendix 31). Note that previously undetected parametric resonance at $b = 0.2$ appears at the higher mass modulation coefficient. This leads to the conclusion that the instability is present even at the larger damping $b > 0.2$, merely on the superior μ.

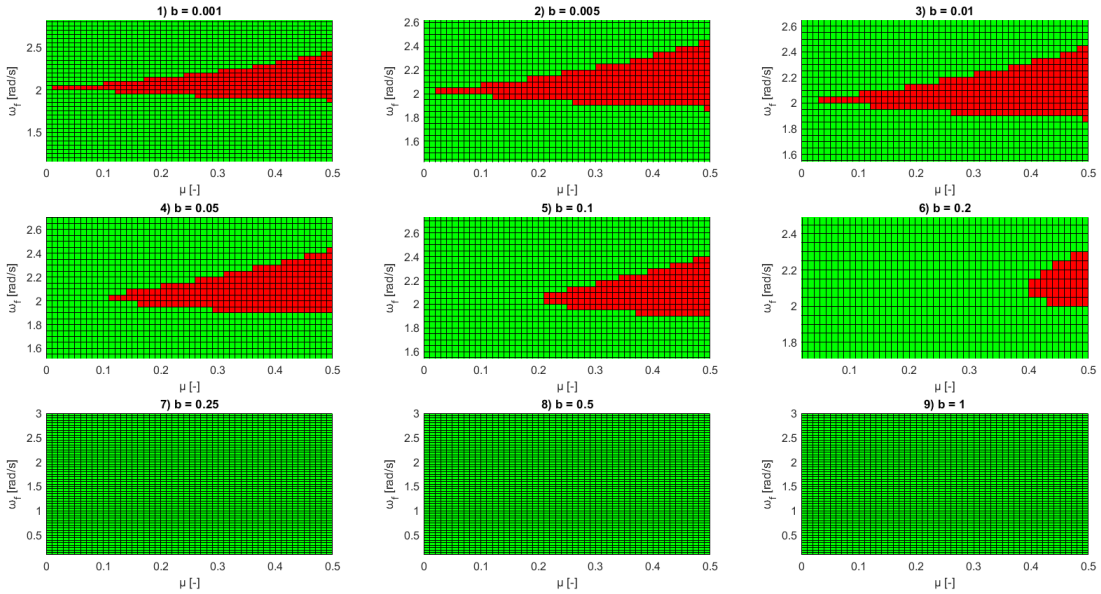

Figure 24: Floquet map for stable (green) and unstable (red) regions of periodic coefficient $(\mu - \omega_f)$

From the Floquet map (Figure 24) the defined points are chosen for a closer check-up (Table 3). The unforced system (66) was running for 200 second in order to determine oscillations' behavior, and further comparison to Floquet analysis. Additionally, the oscillations of the forced system (64) were detected and plotted. The result is presented in Figure 25. The unforced oscillations (66) displayed with blue line and forced (59) - with red.

Table 3: Parameter values and its stability according to Floquet map

	b	μ	ω_f	stability		b	μ	ω_f	stability
1	0.001	0.1	2	*unstable*	10	0.05	0.1	2	*stable*
2	0.001	0.2	2.1	*unstable*	11	0.05	0.2	2.1	*unstable*
3	0.001	0.45	2.2	*unstable*	12	0.05	0.45	2.2	*unstable*
4	0.005	0.1	2	*unstable*	13	0.1	0.1	2	*stable*
5	0.005	0.2	2.1	*unstable*	14	0.1	0.2	2.1	*stable*
6	0.005	0.45	2.2	*unstable*	15	0.1	0.45	2.2	*unstable*
7	0.01	0.1	2	*unstable*	16	0.2	0.1	2	*stable*
8	0.01	0.2	2.1	*unstable*	17	0.2	0.2	2.1	*stable*
9	0.01	0.45	2.2	*unstable*	18	0.2	0.45	2.2	*unstable*

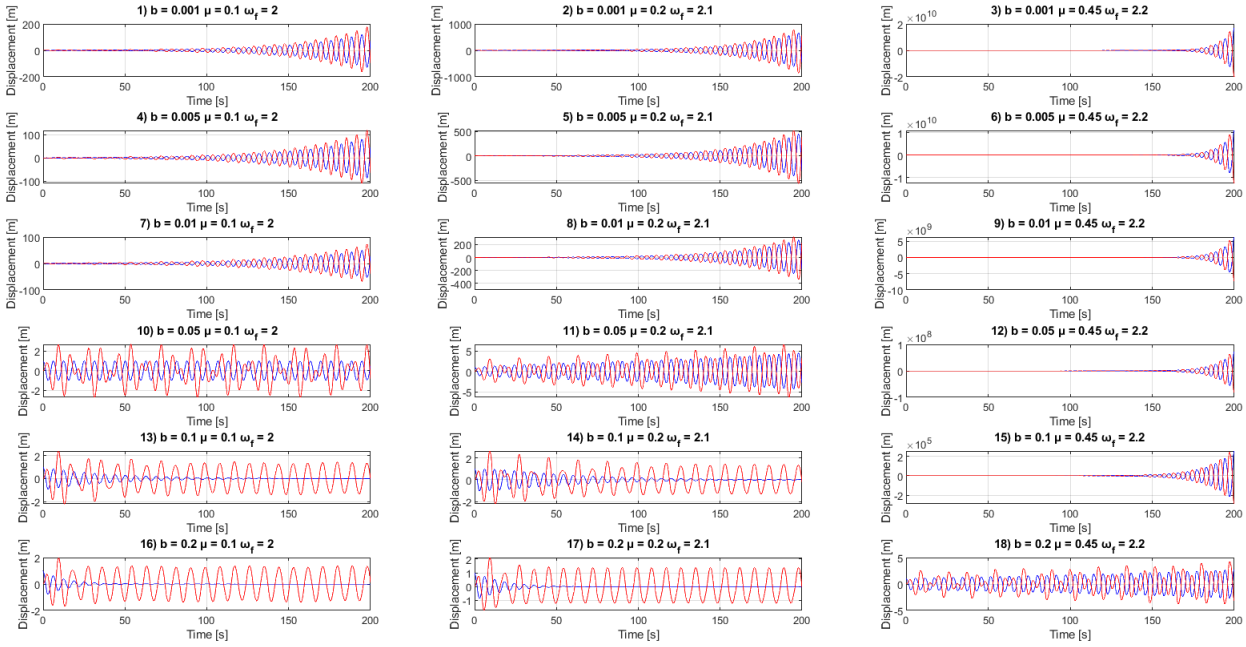

Figure 25: Forced (red) and unforced (blue) oscillations at designated $(\mu - \omega_f)$ points

Figure 25 proves that the unforced system has the same stable/unstable regions as in the Floquet map. Moreover, the stability regions of the forced system are inevitable due to the forcing element. However, at some points, e.g. 18, the stability mode is not certain looking at Figure 25, therefore a higher simulation time is required to detect parametric resonance (Figure 26). This comes at the cost of complexity of simulations and accuracy of results, which has to be decreased in order to finish the simulation.

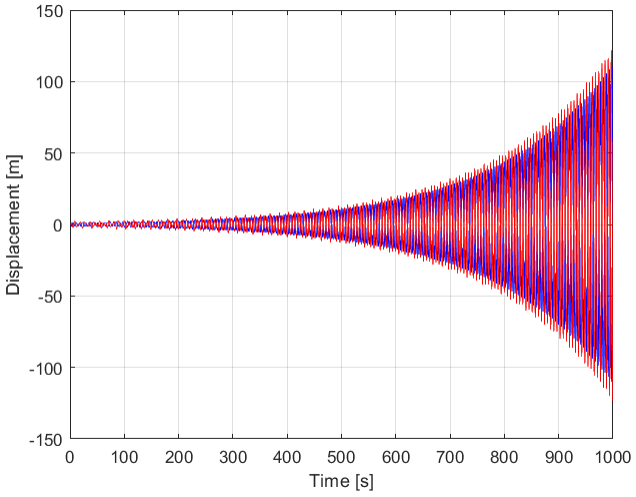

Figure 26: Forced (red) and unforced (blue) oscillations within 1000 seconds running time at $\mu = 0, 2$ and $\omega_f = 2.2$

5 Conclusion

In this work, the phenomenon of parametric resonance was utilized to increase the performance of the WEC. Despite that the phenomenon was discovered in the 19th century, its application in the WEC devices is a relatively new concept. Few studies have been made suggesting mass modulation as a periodic parameter in the WEC system. The mass modulation would happen using the ambient water, the fluid capture and release would happen evenly twice per natural period of the system. The WEC is a complex device, that has lots of non-linear terms. However, at the earlier step, the simplified mass-spring-damper model can be used, where the damper is representing PTO. Based on that, the numerical integration and stability diagram for the single DOF model was performed and the power output recorded and inspected.

The power is dependent on the damping: if the damping coefficient is too high, then the motion of the system will be limited, and a small amount of power will be produced, nonetheless, if the damping coefficient is too low, then the damper absorbs little of energy, hence the power capture is lower. Therefore the tuning and optimization methods have been suggested. Overall, the preliminary results show significant improvement of the power rate at parametric resonance compares to other cases of parametric oscillations as well as in comparison to the system at resonance. Within the simulations, few regularities have stood out, e.g. that the stability is not affected by forcing term, hence forced and unforced models will have the same outcome if the parameter values are intact. Also, that the system tends to have higher output at the higher modulation coefficient, i.e. more mass (and hence inertia) needs to be added and subtracted from the system over a cycle to increase a power output. However, this improvement is limited by the complexity of the design and realization costs of such model.

The methods used to investigate the performance both have positive and negative points. Due to the simplification of the model, i.e. single DOF, the numerical integration seem easier, as it does not require broad knowledge in linear/non-linear dynamics and stability analysis. This method exploits the technical facilities and presents readable results. However, as the complexity gets closer to an original WEC device, the system will have more non-linear terms and parameters, and those will affect the simulation running time and accuracy of the results. Also, with borderline cases, shown in Floquet map, e.g. the oscillations in Figure 26, the necessary time to detect the resonance increases. Further work has to implicate the stability theory along with numerical simulations, where stability map could define the search area and numerical integration at the designated area could define actual results.

The real waters rarely exhibit ordinary conditions, instead, the amplitude of the waves along with their velocity (frequency) changing regularly. The next step in the utilization of parametric resonance in WEC devices would be to increase the number of DOFs and adapt to the wave behavior. Perhaps, a wide range of forcing frequencies have to be used to mimic the irregular nature of the waves.

References

[1] H.-W. Fang, Y.-Z. Feng, and G.-P. Li, "Optimization of wave energy converter arrays by an improved differential evolution algorithm," *Energies*, vol. 11, no. 12, p. 3522, 2018.

[2] A. Babarit, "A database of capture width ratio of wave energy converters," *Renewable Energy*, vol. 80, pp. 610–628, 2015.

[3] J. Tan, H. Polinder, A. J. Laguna, P. Wellens, and S. A. Miedema, "The influence of sizing of wave energy converters on the techno-economic performance," *Journal of Marine Science and Engineering*, vol. 9, no. 1, p. 52, 2021.

[4] J. Davidson and T. Kalmár-Nagy, "A real-time detection system for the onset of parametric resonance in wave energy converters," *Journal of Marine Science and Engineering*, vol. 8, no. 10, p. 819, 2020.

[5] D. D. Forbush, G. Bacelli, S. J. Spencer, and R. G. Coe, "A self-tuning wec controller for changing sea states," *IFAC-PapersOnLine*, vol. 53, no. 2, pp. 12307–12312, 2020.

[6] H. Yavuz, T. Stallard, A. McCabe, and G. A. Aggidis, "Time series analysis-based adaptive tuning techniques for a heaving wave energy converter in irregular seas," *Proceedings of the Institution of Mechanical Engineers, Part A: Journal of Power and Energy*, vol. 221, no. 1, pp. 77–90, 2007.

[7] C. Cargo, A. Hillis, and A. Plummer, "Strategies for active tuning of wave energy converter hydraulic power take-off mechanisms," *Renewable Energy*, vol. 94, pp. 32–47, 2016.

[8] L. Cuadra, S. Salcedo-Sanz, J. Nieto-Borge, E. Alexandre, and G. Rodríguez, "Computational intelligence in wave energy: Comprehensive review and case study," *Renewable and Sustainable Energy Reviews*, vol. 58, pp. 1223–1246, 2016.

[9] W. Froude, "On the rolling of ships.," *Trans INA*, vol. 2, pp. 180–227, 1861.

[10] D. Rugar and P. Grütter, "Mechanical parametric amplification and thermomechanical noise squeezing," *Physical Review Letters*, vol. 67, no. 6, p. 699, 1991.

[11] A. Olvera, E. Prado, and S. Czitrom, "Parametric resonance in an oscillating water column," *Journal of Engineering Mathematics*, vol. 57, no. 1, pp. 1–21, 2007.

[12] B. Orazov, O. O'Reilly, and Ö. Savaş, "On the dynamics of a novel ocean wave energy converter," *Journal of Sound and Vibration*, vol. 329, no. 24, pp. 5058–5069, 2010.

[13] B. Orazov, O. M. O'Reilly, and X. Zhou, "On forced oscillations of a simple model for a novel wave energy converter," *Nonlinear Dynamics*, vol. 67, no. 2, pp. 1135–1146, 2012.

[14] A. Kahan, "Global electricity consumption continues to rise faster than population." `https://www.eia.gov/todayinenergy/detail.php?id=44095#`. Accessed: 2020-06-15.

[15] R. Roesch, F. Boshell, E. Ocenic, A. Salgado, J. Hecke, G. Castellanos, D. Gielen, M. Abunofal, S. Ratka, and A. Abdel-Latif, "Fostering a blue economy: Offshore renewable energy," 2020.

[16] L. Mofor, J. Goldsmith, and F. Jones, "Ocean energy: Technology readiness, patents, deployment status and outlook," *Abu Dhabi*, 2014.

[17] A. Clément, P. McCullen, A. Falcão, A. Fiorentino, F. Gardner, K. Hammarlund, G. Lemonis, T. Lewis, K. Nielsen, S. Petroncini, *et al.*, "Wave energy in europe: current status and perspectives," *Renewable and sustainable energy reviews*, vol. 6, no. 5, pp. 405–431, 2002.

[18] B. E. Layton, "A comparison of energy densities of prevalent energy sources in units of joules per cubic meter," *International Journal of Green Energy*, vol. 5, no. 6, pp. 438–455, 2008.

[19] J. Leishman and G. Scobie, "The development of wave power: a techno-economic study," 1976.

[20] B. KOYUNCU, M. MAHMOOD, and I. MYDERRIZI, "Theory and applications of wave energy converters: A review,"

[21] T. W. Thorpe *et al.*, *A brief review of wave energy*. Harwell Laboratory, Energy Technology Support Unit London, 1999.

[22] E. Ocean Yearbook Online, "Oceans and the law of the sea report of the secretary-general, 2019," *Ocean Yearbook Online*, vol. 34, no. 1, pp. 651–675.

[23] Y. Sang, H. B. Karayaka, Y. Yan, N. Yilmaz, and D. Souders, "1.18 ocean (marine) energy," 2018.

[24] T. Aderinto and H. Li, "Review on power performance and efficiency of wave energy converters," *Energies*, vol. 12, no. 22, p. 4329, 2019.

[25] R. Pelc and R. M. Fujita, "Renewable energy from the ocean," *Marine Policy*, vol. 26, no. 6, pp. 471–479, 2002.

[26] J. Falnes, "A review of wave-energy extraction," *Marine structures*, vol. 20, no. 4, pp. 185–201, 2007.

[27] B. Drew, A. R. Plummer, and M. N. Sahinkaya, "A review of wave energy converter technology," *Proceedings of the Institution of Mechanical Engineers, Part A: Journal of Power and Energy*, vol. 223, no. 8, pp. 887–902, 2009.

[28] G. Mork, S. Barstow, A. Kabuth, and M. T. Pontes, "Assessing the global wave energy potential," in *International Conference on Offshore Mechanics and Arctic Engineering*, vol. 49118, pp. 447–454, 2010.

[29] I. Dincer, *Comprehensive energy systems*. Elsevier, 2018.

[30] R. Kempener and F. Neumann, "Tidal energy technology brief," *International Renewable Energy Agency (IRENA)*, pp. 1–34, 2014.

[31] T. Aderinto and H. Li, "Ocean wave energy converters: Status and challenges," *Energies*, vol. 11, no. 5, p. 1250, 2018.

[32] F. d. O. Antonio, "Wave energy utilization: A review of the technologies," *Renewable and sustainable energy reviews*, vol. 14, no. 3, pp. 899–918, 2010.

[33] B. K. Hodge, *Alternative energy systems and applications*. John Wiley & Sons, 2017.

[34] M. R. Houhou, S. S. Dol, M. S. Khan, and A. A. Azeez, "Feasibility study on converting ocean waves energy by pelamis in united arab emirates," in *2018 Advances in Science and Engineering Technology International Conferences (ASET)*, pp. 1–5, IEEE, 2018.

[35] R. Yemm, "The history and status of the pelamis wave energy converter," in *Wave power–Moving towards commercial viability", IMECHE Seminar, London, UK*, 1999.

[36] T. Whittaker, W. Beattie, M. Folley, C. Boake, A. Wright, M. Osterried, and T. Heath, "The limpet wave power project—the first years of operation," *Renewable Energy*, 2004.

[37] B. Czech and P. Bauer, "Wave energy converter concepts: Design challenges and classification," *IEEE Industrial Electronics Magazine*, vol. 6, no. 2, pp. 4–16, 2012.

[38] H. Polinder and M. Scuotto, "Wave energy converters and their impact on power systems," in *2005 International Conference on Future Power Systems*, pp. 9–pp, IEEE, 2005.

[39] M. Leijon, O. Danielsson, M. Eriksson, K. Thorburn, H. Bernhoff, J. Isberg, J. Sundberg, I. Ivanova, E. Sjöstedt, O. Ågren, *et al.*, "An electrical approach to wave energy conversion," *Renewable energy*, vol. 31, no. 9, pp. 1309–1319, 2006.

[40] C. A. Diamond, C. Q. Judge, B. Orazov, Ö. Savaş, *et al.*, "Mass-modulation schemes for a class of wave energy converters: Experiments, models, and efficacy," *Ocean Engineering*, vol. 104, pp. 452–468, 2015.

[41] K. Billah, "On the definition of parametric excitation for vibration problems," *Journal of Sound Vibration*, vol. 270, no. 1-2, pp. 450–454, 2004.

[42] E. I. Butikov, "Parametric resonance in a linear oscillator at square-wave modulation," *European journal of physics*, vol. 26, no. 1, p. 157, 2004.

[43] D. Watt and M. Cartmell, "An externally loaded parametric oscillator," *Journal of sound and vibration*, vol. 170, no. 3, pp. 339–364, 1994.

[44] C. A. Diamond, O. M. O'Reilly, and Ö. Savaş, "The impulsive effects of momentum transfer on the dynamics of a novel ocean wave energy converter," *Journal of Sound and Vibration*, vol. 332, no. 21, pp. 5559–5565, 2013.

[45] A. Nayfeh and D. Mook, "Nonlinear oscillations, john wiley & sons, new york," *1979*, 1979.

[46] A. Stanford and J. Tanner, "8 - oscillations," in *Physics for Students of Science and Engineering* (A. Stanford and J. Tanner, eds.), pp. 210–233, Academic Press, 1985.

[47] T. Fossen and H. Nijmeijer, *Parametric resonance in dynamical systems*. Springer Science & Business Media, 2011.

[48] M. Faraday, "On a peculiar class of acoustical figures; and on certain forms assumed by groups of particles upon vibrating elastic surfaces," in *Abstracts of the Papers Printed in the Philosophical Transactions of the Royal Society of London*, no. 3, pp. 49–51, The Royal Society London, 1837.

[49] C. Holden, R. Galeazzi, C. Rodríguez, T. Perez, T. I. Fossen, M. Blanke, M. de Almeida, and S. Neves, "Nonlinear container ship model for the study of parametric roll resonance," 2007.

[50] B. Van Laarhoven, "Stability analysis of parametric roll resonance," *Eindhoven University of Technology Department Mechanical Engineering Dynamics and Control Group Eindhoven*, 2009.

[51] H. Davies, "Parametric rolling motion – a twist in the tail!." `https://www.stratumfive.com/industry/parametric-rolling-motion-prm-contributes-to-the-loss-of-around-1000-containers-a-` Accessed: 2020-11-25.

[52] C. Holden, R. Galeazzi, T. I. Fossen, and T. Perez, "Stabilization of parametric roll resonance with active u-tanks via lyapunov control design," in *2009 European Control Conference (ECC)*, pp. 4889–4894, IEEE, 2009.

[53] N. Umeda, H. Hashimoto, S. Minegaki, and A. Matsuda, "An investigation of different methods for the prevention of parametric rolling," *Journal of marine science and technology*, vol. 13, no. 1, pp. 16–23, 2008.

[54] R. Galeazzi and K. Y. Pettersen, "Controlling parametric resonance: Induction and stabilization of unstable motions," in *Parametric Resonance in Dynamical Systems*, pp. 305–327, Springer, 2012.

[55] J. B. Rho, H. S. Choi, H. S. Shin, I. K. Park, *et al.*, "A study on mathieu-type instability of conventional spar platform in regular waves," *International Journal of Offshore and Polar Engineering*, vol. 15, no. 02, 2005.

[56] J. P. Ortiz, *The influence of mooring dynamics on the performance of self reacting point absorbers*. PhD thesis, 2016.

[57] R. Gomes, J. Ferreira, S. R. de Silva, J. Henriques, and L. Gato, "An experimental study on the reduction of the dynamic instability in the oscillating water column spar buoy," in *Proceedings of the 12th European Wave and Tidal Energy Conference, Cork, Ireland*, vol. 27, 2017.

[58] É. Mathieu, "Mémoire sur le mouvement vibratoire d'une membrane de forme elliptique.," *Journal de mathématiques pures et appliquées*, vol. 13, pp. 137–203, 1868.

[59] B. van der Pol and M. Strutt, "Ii. on the stability of the solutions of mathieu's equation," *The London, Edinburgh, and Dublin Philosophical Magazine and Journal of Science*, vol. 5, no. 27, pp. 18–38, 1928.

[60] D. J. Daniel, "Exact solutions of mathieu's equation," *Progress of Theoretical and Experimental Physics*, vol. 2020, no. 4, p. 043A01, 2020.

[61] R. H. Rand, "Lecture notes on nonlinear vibrations," 2012.

[62] L. Turyn, "The damped mathieu equation," *Quarterly of applied mathematics*, vol. 51, no. 2, pp. 389–398, 1993.

[63] A. H. Nayfeh, *Introduction to perturbation techniques*. John Wiley & Sons, 2011.

[64] J. R. Carson, "Notes on the theory of modulation," *Proceedings of the Institute of Radio Engineers*, vol. 10, no. 1, pp. 57–64, 1922.

[65] W. Barrow, "On the oscillations of a circuit having a periodically varying capacitance," *Proceedings of the Institute of Radio Engineers*, vol. 22, no. 2, pp. 201–212, 1934.

[66] B. Epstein and R. Barakat, "Perturbation solutions of the carson–cambi equation," *Journal of the Franklin Institute*, vol. 303, no. 2, pp. 177–188, 1977.

[67] P. Pedersen, "A quantitative stability analysis of the solutions to the carson-cambi equation," *Journal of the Franklin Institute*, vol. 309, no. 5, pp. 359–367, 1980.

[68] P. Pedersen, "Stability of the solutions to mathieu-hill equations with damping," *Ingenieur-Archiv*, vol. 49, no. 1, pp. 15–29, 1980.

[69] N. P. Reeves, J. Cholewicki, J. H. Van Dieën, G. Kawchuk, and P. W. Hodges, "Are stability and instability relevant concepts for back pain?," *journal of orthopaedic & sports physical therapy*, vol. 49, no. 6, pp. 415–424, 2019.

[70] K. Kuttler, "An introduction to linear algebra," *Brigham Young University: Provo, UT, USA*, 2007.

[71] A. P. Seyranian and A. A. Mailybaev, *Multiparameter stability theory with mechanical applications*, vol. 13. World Scientific, 2003.

[72] A. M. Vinogradov and B. A. Kupershmidt, "The structures of hamiltonian mechanics," *Russian Mathematical Surveys*, vol. 32, no. 4, pp. 177–243, 1977.

[73] T. S. Parker and L. O. Chua, "Stability of limit sets," in *Practical Numerical Algorithms for Chaotic Systems*, pp. 57–82, Springer, 1989.

[74] T. S. Parker and L. O. Chua, "Poincaré maps," in *Practical Numerical Algorithms for Chaotic Systems*, pp. 31–56, Springer, 1989.

[75] G. Floquet, "Sur les équations différentielles linéaires à coefficients périodiques," in *Annales scientifiques de l'École normale supérieure*, vol. 12, pp. 47–88, 1883.

[76] R. Grimshaw, *Nonlinear ordinary differential equations*, vol. 2. CRC Press, 1991.

[77] T. Burton and J. Muldowney, "A generalized floquet theory," *Archiv der Mathematik*, vol. 19, pp. 188–194, 04 1968.

[78] C. A. Klausmeier, "Floquet theory: a useful tool for understanding nonequilibrium dynamics," *Theoretical Ecology*, vol. 1, no. 3, pp. 153–161, 2008.

[79] A. Têtu, "Power take-off systems for wecs," in *Handbook of ocean wave energy*, pp. 203–220, Springer, Cham, 2017.

[80] S. H. Salter *et al.*, "Wave power," *Nature*, vol. 249, no. 5459, pp. 720–724, 1974.

[81] C. C. Mei, "Power extraction from water waves," *Journal of ship research*, vol. 20, no. 02, pp. 63–66, 1976.

Appendix

Figure 27: Averaged power distribution due to damping at $\omega = 1$

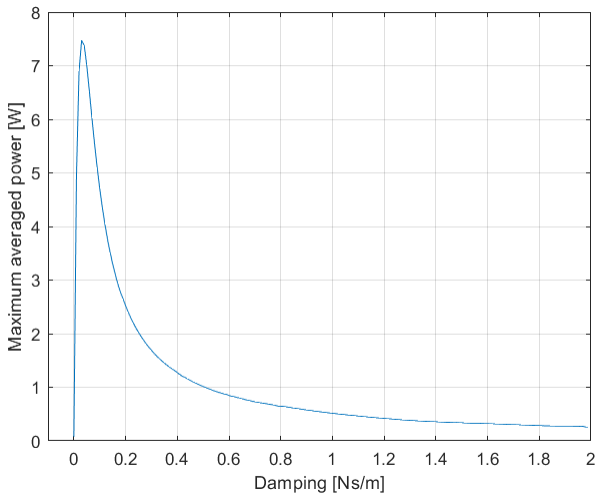

Figure 28: The absolute velocity of the system (64) at different damping b compared to the velocity of common system v

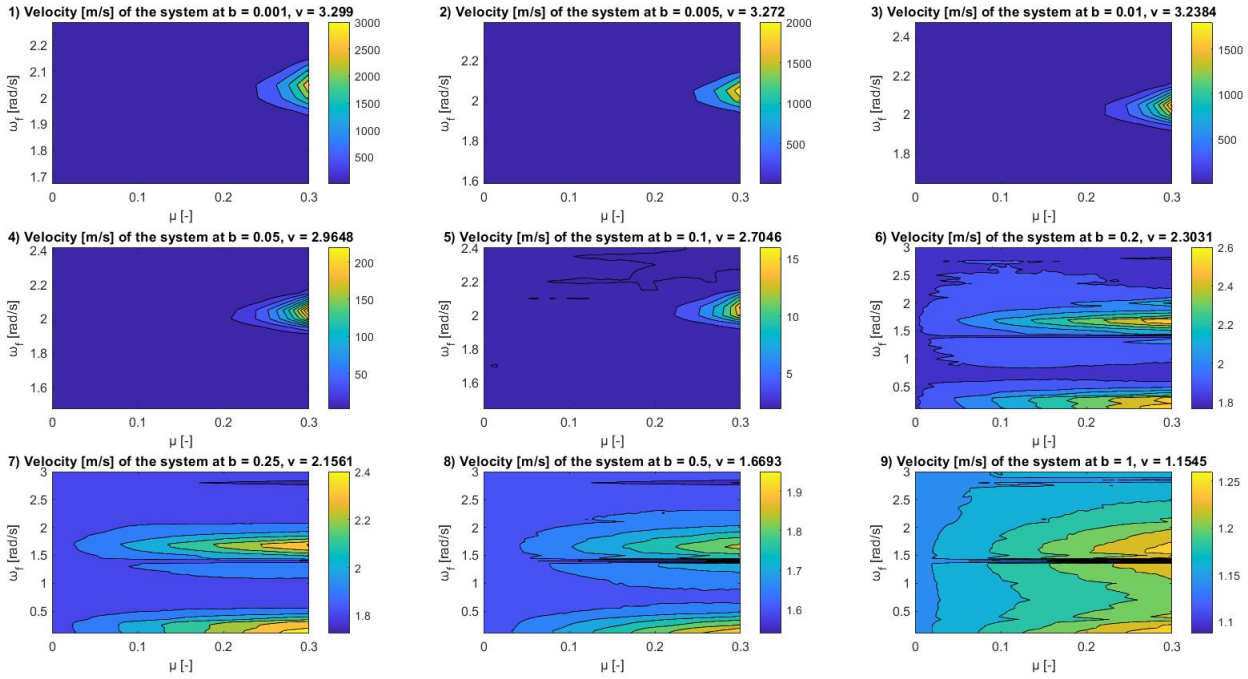

Figure 29: Averaged power distribution due to damping at $\mu = 0.2$ and $\omega_f = 2$

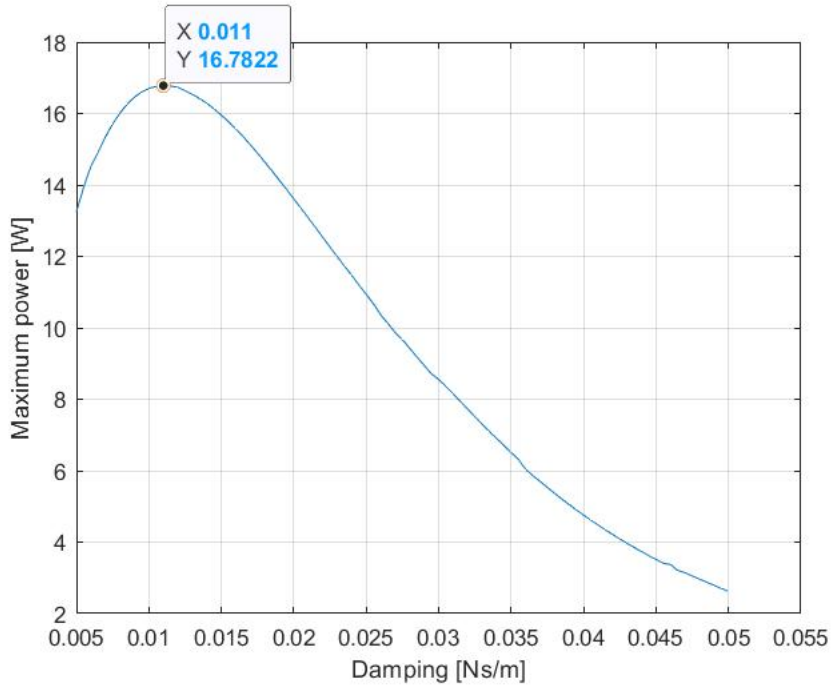

Figure 30: The maximum power output as the system reaches realistic threshold of absolute amplitude $d_{max} = 25$. The power is in log_{10} scale.

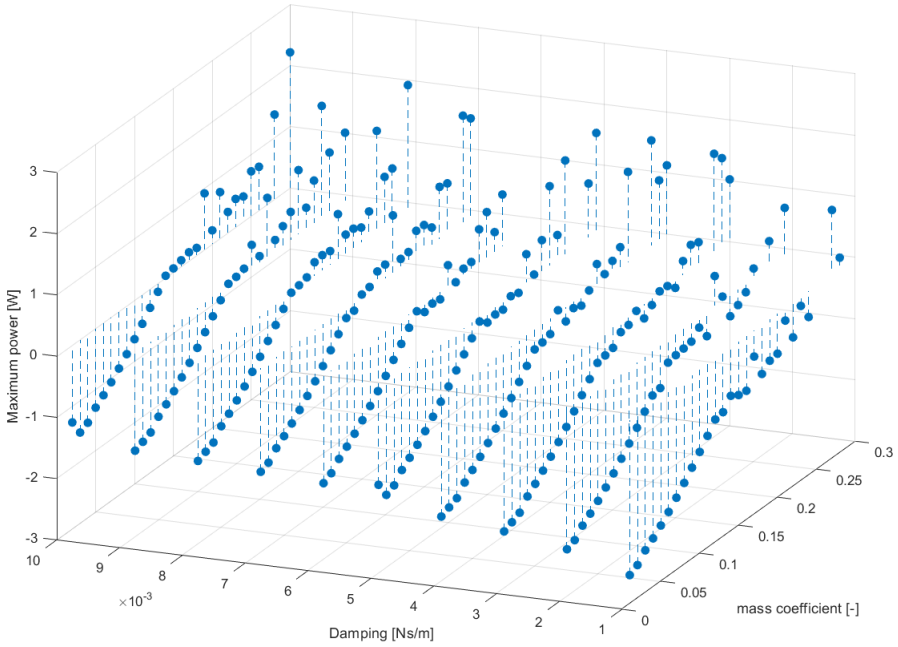

Figure 31: Stability analysis using Floquet theory; stable zones depicted with green and unstable - with red